Cy. 6.

MARTIN MARIETTA ENERGY SYSTEMS LIBRARIES

3 4456 0361332 9

CENTRAL RESEARCH LIBRARY
DOCUMENT COLLECTION

ORNL-2635
Metallurgy and Ceramics

Cy. 6

DEFORMATION TEXTURES IN URANIUM-ALUMINUM ALLOYS

W. C. Thurber

CENTRAL RESEARCH LIBRARY
DOCUMENT COLLECTION
LIBRARY LOAN COPY
DO NOT TRANSFER TO ANOTHER PERSON
If you wish someone else to see this document, send in name with document and the library will arrange a loan.

OAK RIDGE NATIONAL LABORATORY
operated by
UNION CARBIDE CORPORATION
for the
U.S. ATOMIC ENERGY COMMISSION

LEGAL NOTICE

This report was prepared as an account of Government sponsored work. Neither the United States, nor the Commission, nor any person acting on behalf of the Commission:

A. Makes any warranty or representation, express or implied, with respect to the accuracy, completeness, or usefulness of the information contained in this report, or that the use of any information, apparatus, method, or process disclosed in this report may not infringe privately owned rights; or

B. Assumes any liabilities with respect to the use of, or for damages resulting from the use of any information, apparatus, method, or process disclosed in this report.

As used in the above, "person acting on behalf of the Commission" includes any employee or contractor of the Commission to the extent that such employee or contractor prepares, handles or distributes, or provides access to, any information pursuant to his employment or contract with the Commission.

UNCLASSIFIED ORNL-2635

Contract No. W-7405-eng-26

METALLURGY DIVISION

DEFORMATION TEXTURES IN URANIUM-ALUMINUM ALLOYS

William Clarence Thurber

DATE ISSUED

NOV 4 1958

Submitted as a Thesis to the Graduate Council of the University of Tennessee in partial fulfillment of the requirements for the degree of Master of Science

OAK RIDGE NATIONAL LABORATORY
Operated by
UNION CARBIDE CORPORATION
for the
Atomic Energy Commission

UNCLASSIFIED

MARTIN MARIETTA ENERGY SYSTEMS LIBRARIES

3 4456 0361332 9

ACKNOWLEDGMENT

The author wishes to especially thank Dr. C. J. McHargue for his advice and assistance throughout the course of the investigation. Thanks are also due to both Dr. McHargue and Dr. E. E. Stansbury for their invaluable assistance in preparing this manuscript.

The author was privileged to be able to perform the experimental work at the Oak Ridge National Laboratory and avail himself of direct and indirect contributions from many on the staff of the Metallurgy Division including G. E. Angel, C. K. H. DuBose, J. C. Ogle, J. B. Flynn, and W. R. Smith.

Finally, the author wishes to express his appreciation to W. D. Mason of the Metallurgy Division's Reports Office for preparation of the finished work.

TABLE OF CONTENTS

CHAPTER		PAGE
I.	SUMMARY	1
II.	INTRODUCTION	3
III.	REVIEW OF PREVIOUS WORK	6
IV.	EXPERIMENTAL PROCEDURES AND EQUIPMENT	15
V.	RESULTS AND DISCUSSION	31
VI.	CONCLUSIONS	58
LIST OF REFERENCES		61

CHAPTER I

SUMMARY

The deformation textures were determined for uranium-aluminum alloys containing up to 13 weight per cent uranium and fabricated by both extrusion and cold rolling. These alloys, which are particularly useful as fuels for nuclear research and testing reactors, contain appreciable quantities of the hard, brittle, intermetallic compound, UAl_4, dispersed in an essentially pure aluminum matrix. The UAl_4 prevents deformation mechanisms, operative in unalloyed aluminum, from acting in the normal manner.

The sheet textures of aluminum, a 5 weight per cent uranium-aluminum alloy, and a 13 weight per cent uranium-aluminum alloy were determined for alloys which were reduced 90 per cent in thickness by cold rolling. The fiber texture of a 13 weight per cent uranium-aluminum alloy that was extruded at 455°C with a 90 per cent reduction in area was also determined.

The most preferred orientations for the cold-rolled aluminum and the cold-rolled 5 weight per cent uranium-aluminum alloy were found to be near $\{113\}\langle\bar{3}\bar{4}3\rangle$ and $\{124\}\langle\bar{2}\bar{3}2\rangle$, respectively. The ideal texture for the cold-rolled 13 weight per cent uranium-aluminum alloy was found to be a near $\langle 111\rangle$ fiber texture. In this alloy, the dispersed intermetallic compound prevented rotations parallel to the rolling plane from occurring and a band of equally preferred directions for the

normal direction existed. The anticipated approach toward a random texture with increasing amounts of dispersed phase was noted.

In the 13 weight per cent uranium-aluminum alloy, extruded at 455°C, a <111> fiber texture was observed. Although complete recrystallization had occurred during deformation, the <100> component ordinarily associated with deformation-induced recrystallization in aluminum was not present. These results indicate that the dispersed phase had prevented normal lattice reorientations from occurring.

CHAPTER II

INTRODUCTION

The deformation textures of metals have been extensively studied because of both the practical implications in metal fabrication and the fundamental knowledge regarding metal behavior that can be gained. Most of these studies have been confined to pure metals or solid-solution alloys and very little attention has been directed toward more complex alloy systems.

The present work is devoted to a study of the deformation textures in uranium-aluminum alloys containing up to 13 weight per cent uranium. As can be seen from the uranium-aluminum constitution diagram in Figure 1, alloys in this range of compositions are characterized by a pure aluminum matrix in which the intermetallic compound, UAl_4, is dispersed. From a fundamental standpoint, this system provides the conditions for studying the effects of a dispersed phase on the textures developed in an essentially pure metal matrix. Further, from a practical standpoint, these alloys are commonly used as fuels for nuclear research and testing reactors. Thus, a thorough study of the deformation textures resulting from rolling and extrusion may lead to the development of improved fabrication procedures.

The deformation textures in sheets of pure aluminum, a 5 weight per cent uranium-aluminum alloy, and a 13 weight per cent uranium-aluminum alloy were determined in the present investigation using specimens which had received a 90 per cent reduction in thickness by

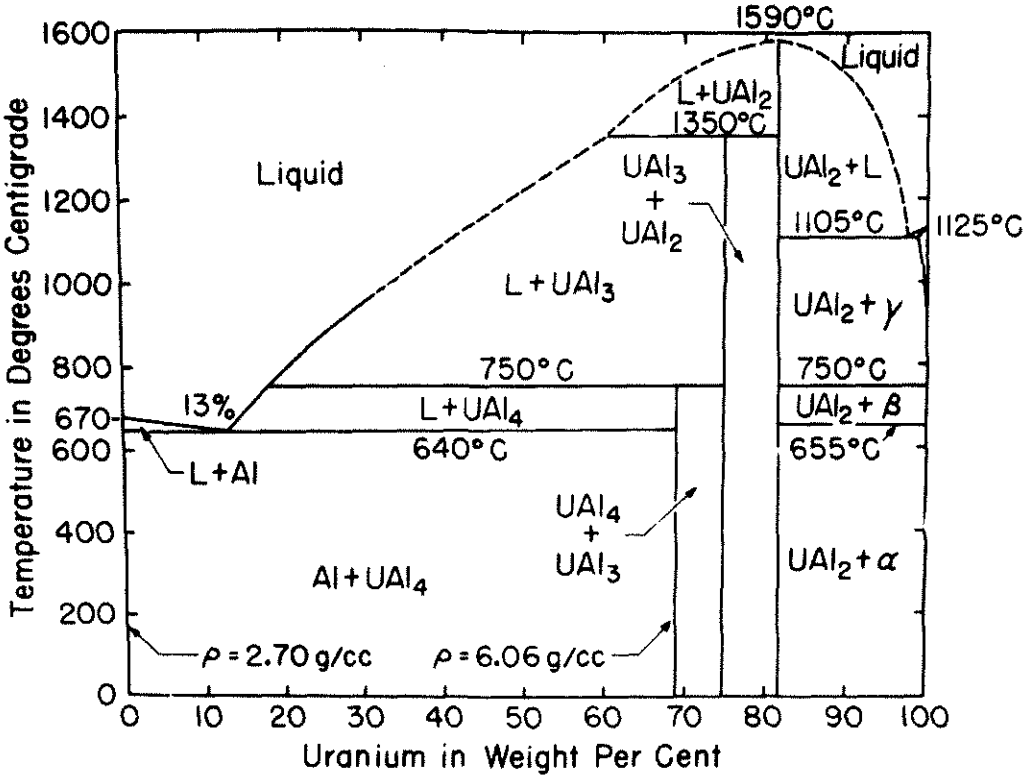

Figure 1 (Y-20808) Aluminum-uranium phase diagram.

cold rolling. The texture in a rod specimen of a 13 weight per cent uranium-aluminum alloy, which had been extruded at 455°C with a 90 per cent reduction in area, was also determined and compared with the fiber texture for pure aluminum extruded under similar conditions.

It can be seen from Figure 1 that the 5 weight per cent uranium-aluminum alloy is a hypoeutectic composition containing 7.3 weight per cent or 3.4 volume per cent UAl_4, while the 13 weight per cent uranium-aluminum alloy is a eutectic composition material containing 18.9 weight per cent or 9.4 volume per cent UAl_4 dispersed in an aluminum matrix.

The textures in all these specimens were determined by a quantitative x-ray spectrometer technique, employing spherical diffraction specimens and a special goniometer. The data obtained are presented as "inverse" pole figures or axis distribution charts rather than as conventional pole figures.

CHAPTER III

REVIEW OF PREVIOUS WORK

When metals are plastically deformed, the individual grains tend to become oriented in a special and reproducible manner wherein certain crystallographic directions become aligned with the directions of principal stress. This preferred orientation is characteristic of the mode, amount, and temperature of deformation, as well as, the particular metal being deformed.

Deformation textures are generally classified as fiber or sheet. Fiber textures are produced by swaging, extrusion, drawing, and uniaxial tension or compression. They are characterized by a particular crystallographic direction parallel to the principal stress axis and an infinite number of equally preferred directions perpendicular to the principal stress axis. Sheet textures, on the other hand, are produced by rolling and are the product of a more complex system of deformation stresses. They are generally described in terms of a particular crystallographic direction parallel to the rolling direction and a particular crystallographic plane parallel to the rolling plane.

Compression and Tension Textures

A number of theories have been expostulated to explain the compression and tension textures developed in plastically deformed metals. The underlying philosophy in each of the theories is that the grains

of the polycrystalline metal must cohere even when subjected to severe deformation strains. The principal difference in each theory lies in the number of operative slip systems which are proposed to explain the resultant texture.

One of the most simple hypotheses is that of Schmid and Boas,[1] who suggested that the three most highly stressed slip systems are operative during deformation and that rotations occur until the lattice reaches a stable end orientation. When this stable end orientation is achieved, rotations cancel one another and only simple slip occurs. Application of this theory to face-centered cubic metals accounts for both <100> and <111> components for tensile deformation and the <110> component for compressive deformation.

This theory was subsequently modified by Pickus and Mathewson,[2] who postulated that three or more slip systems are operative in producing the end position. The conditions which must be met to produce this stable orientation include:

1. The slip directions for the operating systems are symmetrically positioned about the stress axis.

2. The value of $\cos \chi \cos \lambda$ must be equal for all the active systems where χ is the angle between the stress axis and the slip plane normal, and λ is the angle between the stress axis and the slip direction.

3. The lattice rotations must cancel one another.

The work of Pickus and Mathewson has been further extended and elaborated upon by Hibbard and Yen.[3] Their rationalization avers that

with a uniaxial tensile stress, stable end orientations are realized when the active slip systems are symmetrically disposed about the stress axis and the active slip directions lie within a space cone 45° from the stress axis. If the active slip directions lie greater than 45° from the stress axis, lattice rotations will occur until a stable end position is reached.

On the basis of this theory, a <111> texture is predicted as the primary texture for drawn wires with <100> allowable though not as probable. Both of these textures will result in maintenance of the circularity of the wire. In pure tension where the cross section need not be maintained as circular, <112> is more favorable than <111>.

In compression, following similar reasoning, the stable end orientations are realized when at least two slip directions lie greater than 45° from the stress axis. Alignment of the <110> with the stress axis is thus predicted as the major compression texture and the <100> alignment is an allowable second texture.

Calnan and Clews[4] have pursued a somewhat different argument in deriving a theory of deformation textures. They propose that the development of textures depends upon the extent to which the direction of the effective stress can move from the direction of the applied stress toward orientations favorable for multiple slip without the critical resolved shear stress being exceeded on the most favorably oriented slip system. This movement is possible in certain grains because the restraint offered by the grain boundaries prevents the resolved effective shear stress from exceeding the critical value.

The effective stress is presumed to move from the applied-stress position along a path perpendicular to contours of relative resolved shear stress for simple slip until a boundary of the unit stereographic triangle is reached. Once the boundary has been reached, the effective stress will move to the <100>, <110>, or <111> where it will remain under the action of multiple slip without rotation.

If the movement of the effective stress axis is sufficiently limited due to the character of the lateral restraints and the effective stress axis does not even rotate to the grain boundary before the critical resolved shear stress is exceeded, then deformation in that grain will occur as simple slip on the only active system and characteristic rotations will occur. In a similar case, but where the effective stress axis has reached a boundary of the stereographic unit triangle before the critical resolved shear stress is exceeded, deformation will be characterized by duplex slip and rotations representative of this more complex slip system will result.

On the basis of this theory, Calnan and Clews predict <100>, <112>, and <111> as end orientations for tensile deformation and <110> as the end orientation for compression. This theory, as does that of Hibbard and Yen, takes issue with the suggestion that the drawing process is identical to pure tensile deformation and proposes that the <111> component is increased at the expense of the <112> component yielding a <111> + <100> duplex texture for cold-drawn wires of face-centered cubic metals.

The actual experimental fiber textures of pure aluminum and most other face-centered cubic metals have been reported as either <111>[5] or duplex <111> + <100>.[6] The resultant texture is generally reported to be independent of the method of wire fabrication whether it is drawing, extruding, rolling, or swaging, although some surface effects peculiar to a particular deformation process may occur.[7] Both the <111> and <100> component are, of course, predicted by the various theories previously discussed.

Hibbard[6] has pointed out that the <100> component of the duplex texture for aluminum results only from intermediate amounts of deformation and being metastable, it should disappear with increasing amounts of reduction. Any <100> component remaining after reductions greater than about 95 per cent, he attributes to room-temperature recrystallization of the high-purity aluminum rather than to deformation.

Further evidence that the <100> component results from recrystallization can be found in the work of McHargue and Jetter,[8] who have demonstrated that faster extrusion speeds and higher extrusion temperatures result in increased amounts of <100> component in high-purity aluminum. For example, in aluminum extruded with a 90 per cent reduction in area at 455°C and an extrusion speed of 0.3 foot per minute, the resulting fiber texture contained 22 per cent <111> and 78 per cent <100> indicating that a major portion of the specimen had recrystallized during deformation, even at this very low extrusion speed.

Sheet Textures

The ideal sheet texture for cold-rolled face-centered cubic metals has been described as $\{110\}\langle\bar{1}12\rangle$[7] where the $\{110\}$ is coincident with the rolling plane and the $\langle\bar{1}12\rangle$ lies in the rolling direction. The formation of this texture is predicated upon two considerations:

1. The only operative slip systems at room temperature are of the form $\{111\}\langle 10\bar{1}\rangle$,[7] that is, slip occurring on the planes of most dense atom packing and in the close-packed direction.

2. Deformation during rolling can be envisioned as the superposition of compressive stresses in the normal direction and tensile stresses in the rolling direction, that is, plane parallelepipedal compression.

Boas and Schmid[1] assume that the rolling plane, $\{110\}$, is determined by pure compression and the rolling direction is the direction which remains stable in tension and also leads to a reduction in sheet thickness. This excludes slip systems in which the slip direction is in the rolling plane or the slip plane is perpendicular to the normal plane. The sheet texture thus predicted is $\{110\}\langle\bar{1}12\rangle$.

Pickus and Mathewson[2] have extended this concept to account for other textures detected during the cold rolling of face-centered cubic metals, again assuming plane parallelepipedal compressions. They propose that the quantity $\cos \chi \cos \lambda \cos \phi$ is a measure of the stability of a given orientation and decreasing values of this function indicate

less stable orientations. (ϕ is the angle between the slip direction and the direction of flow. χ and λ were previously defined.)

On this basis the following sheet textures and their relative stabilities are predicted.

Orientation	Cos χ Cos λ Cos ϕ
$\{110\}\langle\bar{1}12\rangle$	0.354
$\{100\}\langle 001\rangle$	0.289
$\{110\}\langle 001\rangle$	0.289
$\{112\}\langle 11\bar{1}\rangle$	0.224
$\{010\}\langle 101\rangle$	0.204
$\{101\}\langle 10\bar{1}\rangle$	0.204
$\{1\bar{3}1\}\langle 112\rangle$	Unstable
$\{1\bar{1}0\}\langle 111\rangle$	Unstable

The rationalization of Hibbard and Yen[3] previously discussed with regard to tension and compression textures has been extended by them to rolling textures as well. They suggest that, in addition to the three prerequisites for a stable end position established by Pickus and Mathewson, two further considerations should be added:

1. The active slip directions should lie within a space cone of 45° or less to the rolling direction.

2. The deformation should be such as to avoid flow in the transverse directions.

Based on the first of these two additional postulates, the $\{101\}\langle 10\bar{1}\rangle$, $\{010\}\langle 101\rangle$, $\{100\}\langle 001\rangle$, and $\{110\}\langle 001\rangle$ textures predicted by Pickus and Mathewson are demonstrated to be intermediate metastable

orientations. The $\{112\}\langle 11\bar{1}\rangle$ orientation is shown to be metastable on the basis of the second additional postulate leaving only $\{110\}\langle \bar{1}12\rangle$ as the final stable end orientation.

The theory presented by Calnan and Clews also predicts $\{110\}\langle \bar{1}12\rangle$ as the predominant component of the rolling texture. These investigators also postulate that $\{110\}\langle 1\bar{1}1\rangle$ and $\{110\}\langle 001\rangle$ should be present as secondary components. In their treatment of rolling textures, the rolling process is not considered to be simple superposition of tension and compression textures but rather a process in which the end condition for tension and compression are simultaneously satisfied.

Observed rolling textures in polycrystalline metals exhibit wide deviations from the suggested $\{110\}\langle \bar{1}12\rangle$ orientation because of several factors including restraint of grain in the sample by adjacent grains and relative rates of hardening on the latent and active slip systems. In cold-rolled aluminum, for example, the principal orientations have been variously reported as:

$(110)[\bar{1}12] + (112)[11\bar{1}]$,[7]

$(135)[53\bar{3}]$,[9]

$(7, 12, 22)[\bar{8}\bar{4}5]$, or near $(123)[\bar{2}11]$,[10]

$(6, 13, 21)[\bar{4}\bar{3}3]$,[11]

$(123)[1\bar{2}1]$.[12]

It is always found that varying amounts of spread occur from these observed principal orientations and information on the ideal texture consequently must be supplemented with some representation of the

distribution of intensities about the principal orientation to provide a complete picture of the deformation texture. A pole figure plotting the distribution of poles of a diffracting plane with respect to one or more reference axes is commonly used for this purpose.

In alloys containing appreciable quantities of a hard phase dispersed in a ductile matrix, as is the case of uranium-aluminum alloys, it would be anticipated that the development of preferred orientation is inhibited or even eliminated. The presence of the second phase, of course, obstructs lattice rotations and impedes slip on the active systems by increasing the critical resolved shear stress. Evidence of this phenomenon has been found in cold-rolled carbon steel containing Fe_3C as the dispersed phase and in 5 – 10 per cent silicon-aluminum alloys containing eutectiferous silicon as the dispersed phase. In these alloys, the tendency to develop orientations characteristic of the iron or aluminum matrix is reduced or eliminated.[13]

CHAPTER IV

EXPERIMENTAL PROCEDURES AND EQUIPMENT

Specimen Preparation

The alloys required for this study were prepared by open-air induction melting the appropriate charge of high-purity aluminum (99.99 per cent) and uranium, if required, in a graphite crucible. Slab-type graphite molds were used for alloys which were subsequently rolled, and a cylindrical graphite mold was used for the alloy which was subsequently extruded. Analysis of the aluminum melting stock is included in Table I while Table II summarizes pertinent casting conditions for the four alloys investigated.

After cropping the slab castings about 1 inch below the head, the remaining material was cold reduced on a 6 inch by 10 inch two-high mill to a 90 per cent reduction in thickness. The billets were reduced approximately 0.030 inch per pass and were reversed after each pass to develop a texture of maximum definition. Although the uranium-bearing alloys exhibited rather severe edge cracking, they could nevertheless be cold rolled to the desired thickness. Small sheets 1.5 inches long by 0.75 inch wide by 0.1 inch thick were carefully sheared from the center of the rolled plate with the major axis of the sheets parallel to the rolling direction. To obtain a specimen of sufficient thickness for subsequent machining of the desired x-ray diffraction sample, three sheets were then laminated into a single three-ply sandwich by joining

TABLE I

VENDOR'S ANALYSIS OF HIGH-PURITY ALUMINUM MELTING STOCK

Metal	Composition	Weight Per Cent
Cu	-	0.002
Si	-	0.001
Fe	-	0.000
Mg	-	0.001
Mn	-	0.000
Others	-	0.000
Al	-	Balance

TABLE II

CASTING CONDITIONS FOR PREPARATION OF ALLOYS

Ingot	Metal Charge Al grams	Metal Charge U grams	Mold Size	Mold Temperature °C	Pouring Temperature °C
Al	2940	-	5 1/4 in. long x 10 in. deep x 1 in. wide + head	350	750
5 wt % U-Al	2850	150	5 1/4 in. long x 10 in. deep x 1 in. wide + head	350	750
13 wt % U-Al	2697	403	5 1/4 in. long x 10 in. deep x 1 in. wide + head	350	750
13 wt % U-Al (extrusion)	2436	364	3-in. diameter x 7 in. deep	225	700

with an adhesive resin. The pure aluminum specimen was bonded with Bondmaster M-648, a modified epoxy resin supplied through the courtesy of the Rubber and Asbestos Corporation, Bloomfield, New Jersey. The 5 weight per cent uranium-aluminum alloy and the 13 weight per cent uranium-aluminum alloy specimens were bonded with Armstrong A-6 adhesive manufactured by Armstrong Products Company, Warsaw, Indiana. These resins were selected since they could be cured at room temperature, thus, precluding the possibility of recrystallization when curing at slightly elevated temperatures.

The extruded 13 weight per cent uranium-aluminum alloy was prepared from the cylindrical ingot listed in Table II. The upper three inches of the ingot were cropped, yielding an extrusion billet three inches in diameter by four inches long. This billet was preheated to 455°C and extruded on a 700-ton hydraulic press at a speed of 6 feet per minute through a flat-face die producing a 1-inch diameter rod. The billet was upset to 3.125-inches diameter prior to extrusion, resulting in an ultimate extrusion ratio of 9.8 to 1 and a total reduction in area of 90 per cent. The rod was quenched with a water spray as it emerged from the die. This extruded rod was of sufficient cross section to permit machining the x-ray specimen from a small section cut from the center portion without lamination.

Spherical diffraction specimens 0.2 inch in diameter were required for the quantitative x-ray spectrometer technique used in this study. Preparation of such specimens has been discussed by Jetter and Borie[14] and is only briefly summarized here:

1. Turn a stem on the sample using a conventional lathe.

2. Mount the stem in the chuck of a dividing head attached to a vertical milling machine which is fitted with an eccentric boring tool.

3. Cut the sphere by rapidly rotating the boring tool while slowly rotating the dividing head and slowly raising the table of the milling machine.

4. Lap the surface of sphere to remove tool markings.

5. Etch the sphere to remove any surface layers disturbed by machining and lapping.

The machined specimens for sheet texture studies were appropriately marked to designate rolling, normal, and transverse directions, and then the stem was machined away. The sphere, in any desired orientation, could be attached to an artificial stem with beeswax for mounting on the x-ray spectrometer. In this way, one specimen was used for the three principal directions merely by relative positioning of the ball on a stem. Since only one direction, the fiber axis, is needed to delineate the rod textures, the stem on the extruded alloy remained integral with the sphere. A typical specimen of this type is shown in Figure 2.

X-Ray Method

The actual x-ray technique used in the present work was that developed by Jetter, Borie, McHargue, and Williams[11,14] at the Oak

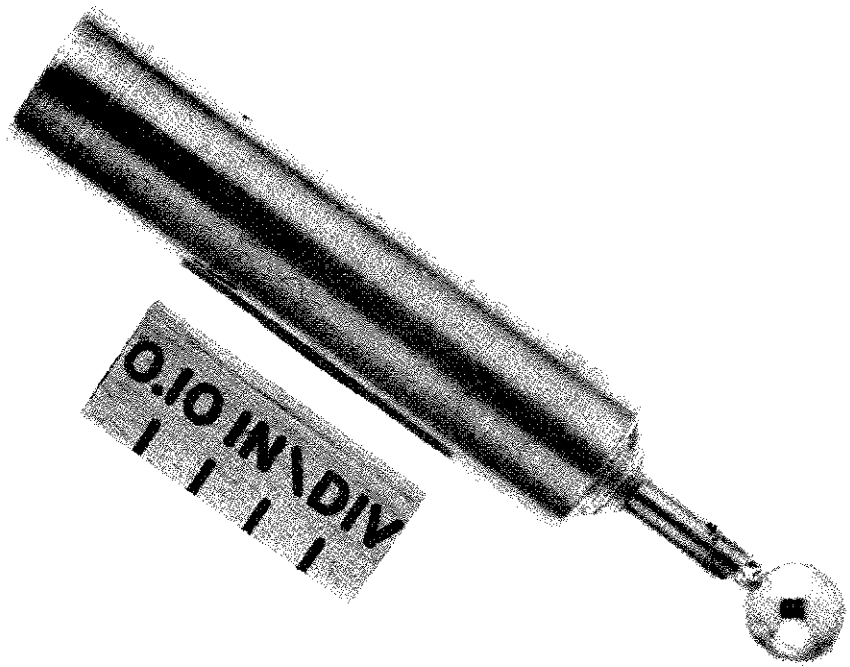

Figure 2 (Y-26596) Spherical x-ray diffraction specimen with stem attached.

Ridge National Laboratory. This is a reflection method employing spherical diffraction specimens. X-ray reflections occur at a given Bragg angle, 2θ, when the specimen is oriented in such a way that the diffraction plane for that Bragg angle is tangent to the surface of the sphere at the point of incidence of the x-ray beam. The spherical diffraction specimen, 0.2 inches in diameter, is mounted in a special goniometer which allows the sphere to be rotated rapidly through an angle, α, about its stem and slowly through an angle, ϕ, about an axis perpendicular to the spectrometer plane while the x-ray source, sphere, and Geiger tube are held in a constant Bragg angle relationship. Rotation through the angle ϕ brings various crystallographic planes of the specimen into tangency with the x-ray beam but reflections will occur only from those planes having $\{h, k, l\}$ for the fixed Bragg angle. The diffraction geometry of this system is illustrated in Figure 3. In the present work the angle, ϕ, was varied from -10° to 90° and the angle, α, was infinite (that is, the ball rotated rapidly and continuously about its stem).

Figure 4 shows the special goniometer with Bodine motors for driving the specimen through the angles α and ϕ. To assure proper alignment of the sphere in this goniometer and in the spectrometer plane, a toolmaker's microscope was used to check the symmetry and position of the sphere for its angular rotations.

The special goniometer pictured in Figure 4 was mounted on the high-angle spectrometer of a North American Phillips x-ray diffractometer. X-radiation, filtered to remove the β component, was obtained

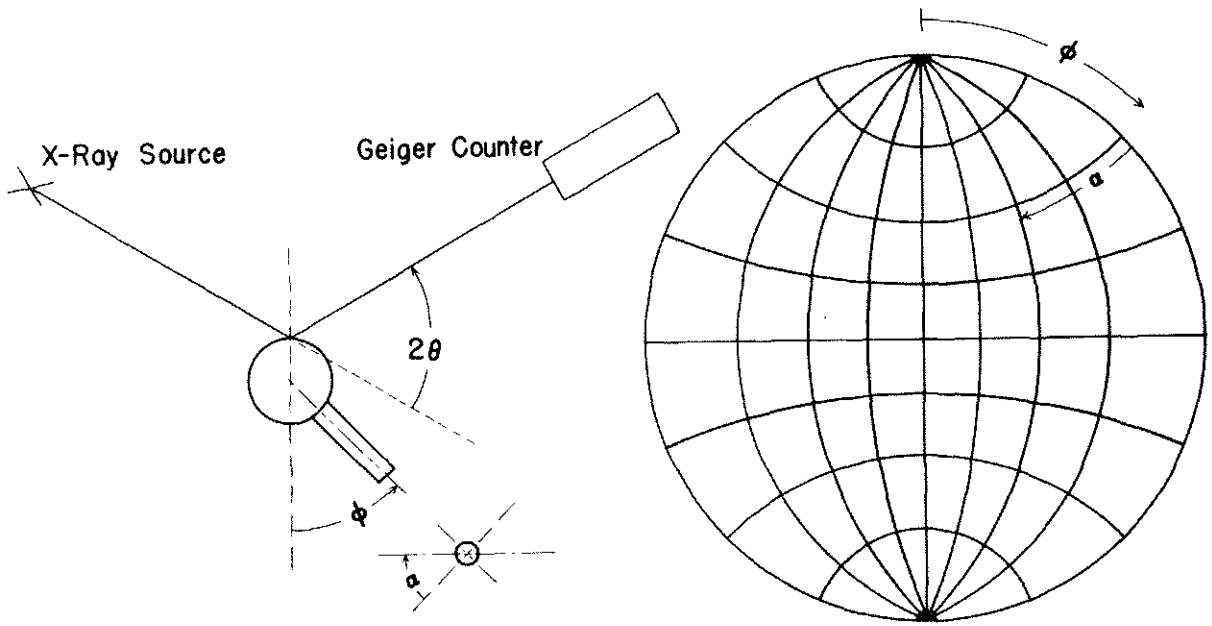

Figure 3 (Y-7688) Diffraction geometry for reflection x-ray technique.

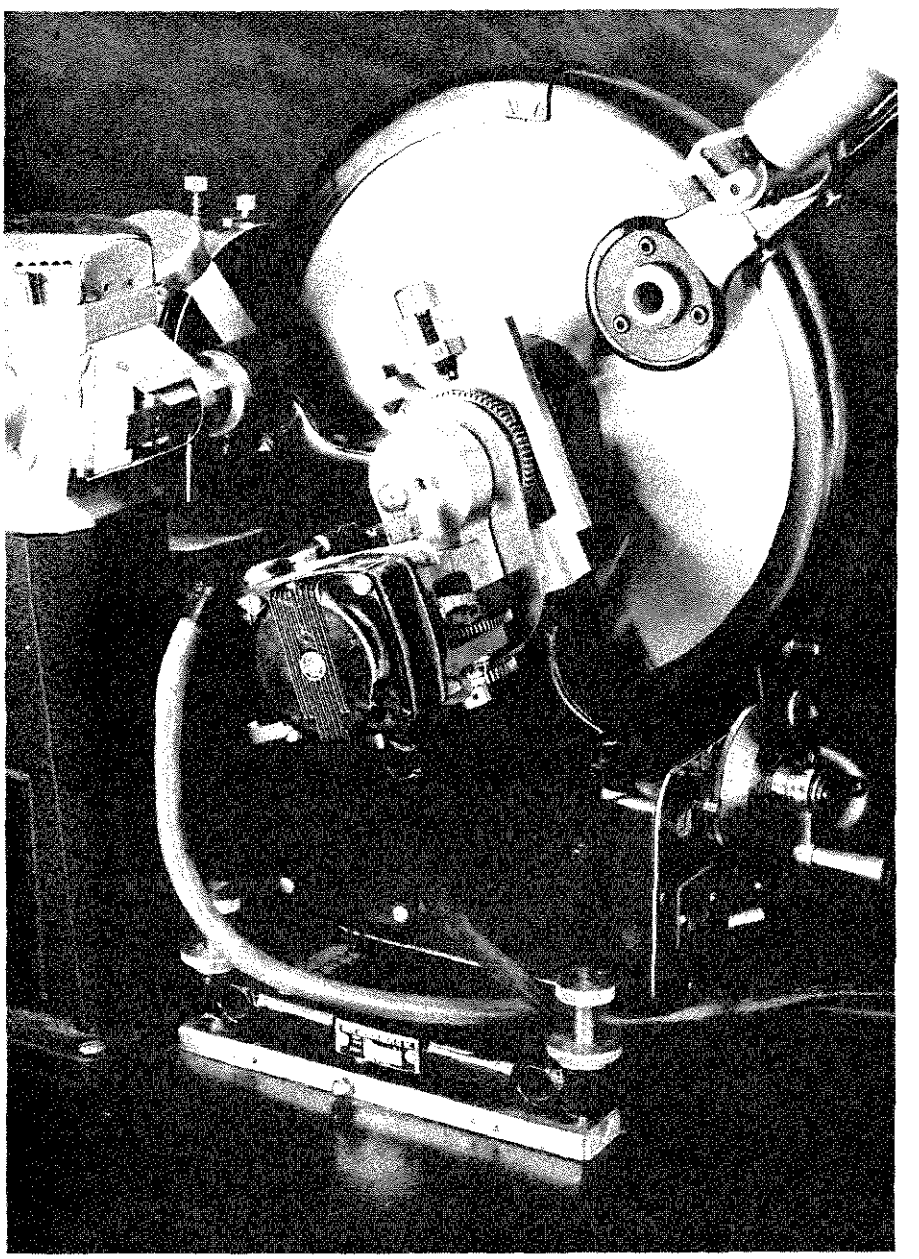

Figure 4 (Y-8628) Special goniometer for producing rotations of spherical diffraction specimens.

from a copper target operated at 35 kilovolts and 20 milliamperes. The incident x-ray beam was collimated through a 1° primary slit and the diffracted beam was collimated through a 1° receiving slit mounted on the counting tube. Although it is generally desirable to use wide angle slits at the Geiger tube, the 1° slit was employed here to minimize interferences from UAl_4 lines in the uranium-bearing specimens. Even so, the diffraction from {015}, {121}, and {114} of UAl_4 occurring at 38.8° caused interference and it was necessary to eliminate the {111} for aluminum from those evaluated. Traces were obtained from only eight crystallographic planes, namely, {200}, {220}, {311}, {400}, {331}, {222}, {422}, and {420}, in the uranium-aluminum alloy specimens.

The procedure for obtaining the trace for a given {h, k, l} is detailed as follows:

1. With the specimen properly aligned in the spectrometer and rotating through α, scan to obtain the 2θ value for maximum intensity for the {h, k, l} in question.

2. Set the Geiger tube at the 2θ for peak intensity.

3. Set the angle, ϕ, of the special goniometer at -10°.

4. Simultaneously actuate ϕ-drive motor and Brown recorder chart and obtain a trace of the angle, ϕ, versus intensity, $I(\phi)$, for the particular value of {h, k, l} scanning from $\phi = -10°$ to $\phi = +90°$.

5. When the ϕ-scan has been completed, set 2θ at a location sufficiently off the peak to give the background intensity. Repeat the ϕ-scan over the same chart to obtain the background intensity.

6. Check this background intensity by running 2θ scans from just below to just above the peak at several constant values of ϕ.

The advantages of the x-ray technique employed here over that conventionally used in determining pole figures include the following:

a. Since this is a reflection method, it is adaptable to metals with high mass-absorption coefficients.

b. Since the geometry does not change, no intensity corrections are required.

c. Only one specimen is necessary for determination of a complete pole figure.

d. Normalization of the data can be accomplished without recourse to a random sample.

Interpretation of X-Ray Data

To properly utilize the x-ray intensity data [$I(\phi)$ versus ϕ], it is first necessary to normalize the data in order to negate the effects of varying multiplicities of the several $\{h, k, l\}$ and to eliminate inherent day-to-day variations in the x-ray technique. Only when the data have been normalized can meaningful intensity comparisons be made. Most x-ray techniques require the use of a random powder sample as a standard of comparison in the normalization process. However, it has been shown[11] that the normalization factor, I_{random}, for the present technique is equal to the area under the curve of $I \sin \phi$ versus ϕ and can be represented symbolically as:

$$I_{random} = \int_{0}^{\pi/2} I(\phi) \sin \phi \, d\phi. \tag{1}$$

Thus, normalization can be achieved merely by evaluation of the integral without recourse to a random sample. Typical plots of $I(\phi)$ versus ϕ and $I(\phi) \sin \phi$ versus ϕ are shown in Figure 5. Graphical integration of the area under the curve in Figure 5b can be readily employed to determine the normalization factor. The normalized intensity, R, at any value of ϕ can be determined by dividing the measured intensity at ϕ by the normalization factor

$$R(\phi) = \frac{I(\phi)}{I_{random}} . \tag{2}$$

Plots of $R(\phi)$, the normalized intensity, can then be made. These plots are actually pole distribution charts showing the distribution of diffracting plane poles relative to a reference axis. A more desirable way of representing the data is to show the distribution of the reference axis relative to a set of standard crystallographic axes.

Jetter, McHargue, and Williams[11] have also shown that the normalized diffraction intensity, R, for given values of $\{h, k, l\}$ and ϕ, is equal to the average value of the normalized axis density, T, along a path ϕ degrees from the diffracting plane pole or

$$R(\phi) = \overline{T}(\phi). \tag{3}$$

This path ϕ degrees from the pole is said to have a total length of $\beta_{maximum}$.

For example, the path $0\text{-}\beta_{maximum}$ for the point shown in Figure 5a at $\phi = 60°$ is plotted on standard stereographic triangle in

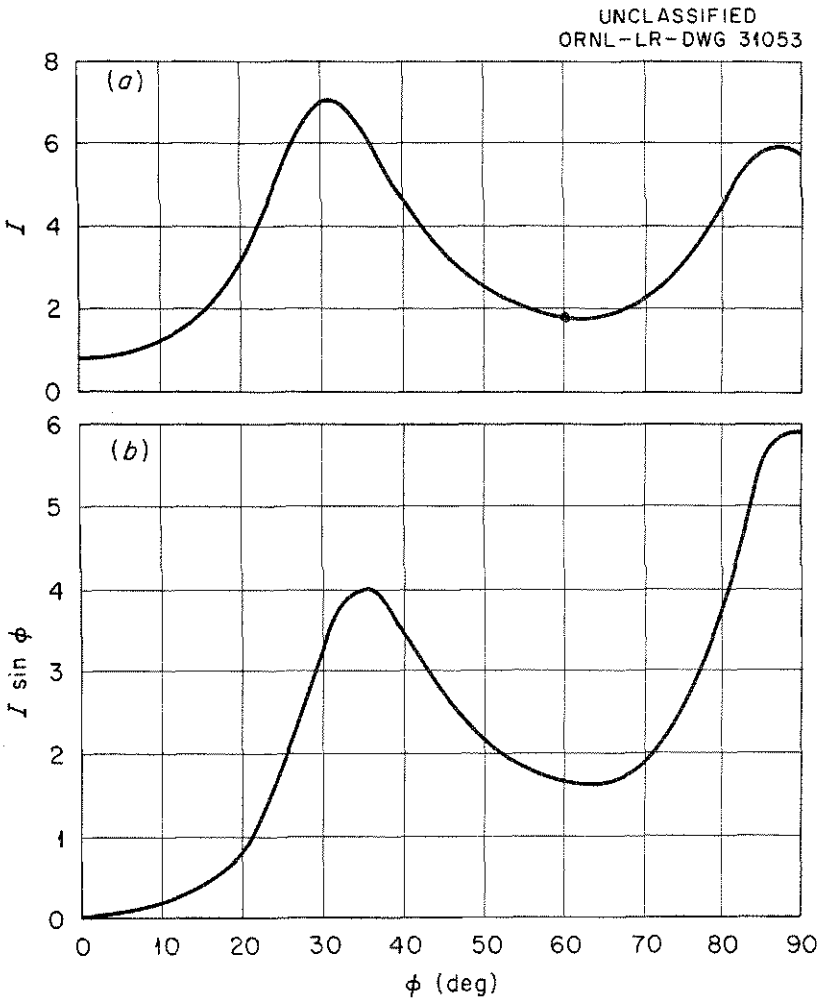

Figure 5. (a) Pole distribution chart for {220} plane for 13 weight per cent uranium-aluminum alloy extruded at 455°C to a 90 per cent reduction in area. The texture is essentially pure <111>. (b) Data from (a) replotted as I sin ϕ versus ϕ.

Figure 6. The value of the normalized axis density averaged over this path is then equal to $R(\phi = 60°)$.

Turning to the actual processing of the x-ray data, a smooth curve was first drawn through the strip chart data for the particular $\{h, k, l\}$ being studied and the background was subtracted yielding the actual intensity, $I(\phi)$, as a function of degrees ϕ. The data were transposed to ordinary graph paper and plots were prepared of $I(\phi)$ versus ϕ and $I(\phi) \sin \phi$ versus ϕ by determining I at 2° intervals from the recorder strip chart. Typical charts of this type were previously shown in Figure 5. Plinimetric measurement was used to obtain a value of the normalization factor from $I \sin \phi$ plot.

The significance of the peaks on a plot of $I(\phi)$ versus ϕ may be interpreted in the following light: If, for a given $\{h, k, l\}$, a peak on the plot occurs at $\phi = 0°$, then the $\{h, k, l\}$ lies perpendicular to the specimen axis under consideration. If $\{h, k, l\}$ is $\{111\}$, then a peak would also be found at $\phi = 70°32'$ since this is the angle between $\{111\}$. A peak on the same plot at $\phi = 54°44'$ would result from $\{100\}$ being perpendicular to the specimen axis and the peak at this location would be caused by the four $\{111\}$ which were symmetrically distributed about $\{100\}$ at $\phi = 0°$.

Actual plotting of the "inverse" pole figure from the pole distribution charts completes the texture determination. Since, at $\phi = 0°$, the normalized axis density, T, is averaged over a point rather than a path of some finite length,

$$\overline{T}(\phi = 0) = T(\phi = 0); \tag{4}$$

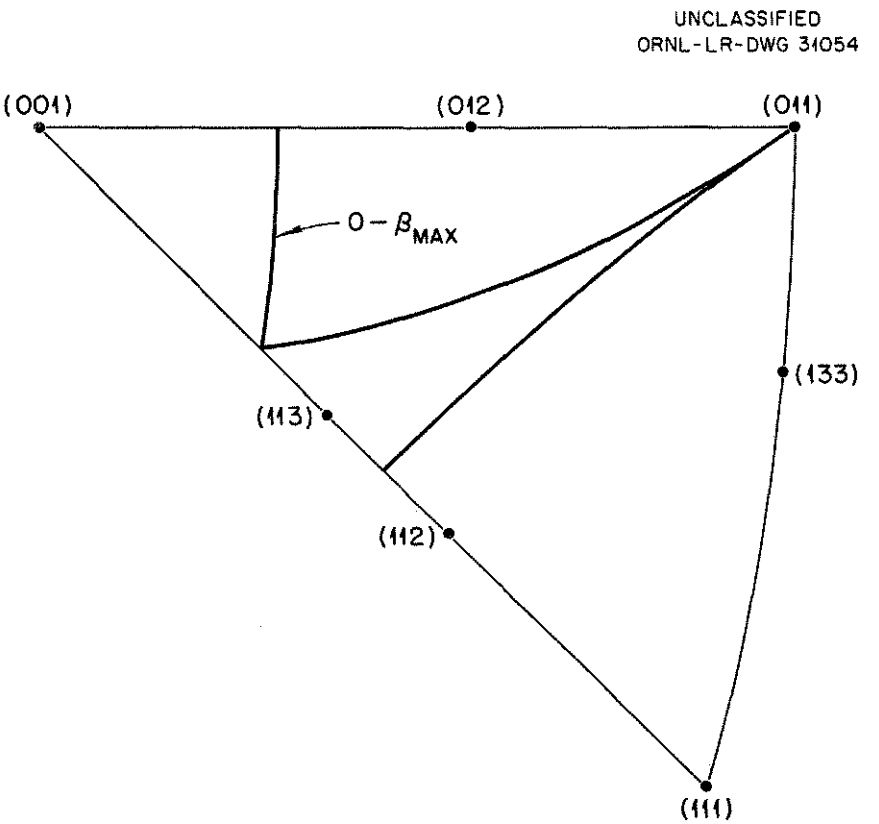

Figure 6. Standard (001) stereographic triangle showing path $0\text{-}\beta_{max}$ for $\phi = 60°$ and $\{h, k, l\} = \{011\}$.

and therefore,

$$T(\phi = 0) = R(\phi = 0). \tag{5}$$

Thus, an unambiguous solution can be realized at seven points on the standard crystallographic triangle simply by calculating $R(\phi = 0)$ for the seven separate crystallographic planes for which intensity traces were obtained. Using these points and pole distribution charts of $R(\phi)$ versus ϕ which were calculated for $\{400\}$, $\{220\}$, and $\{222\}$, a solution was assumed by sketching intensity contours on a standard stereographic triangle. This solution was checked using special charts plotting the path $0\text{-}\beta_{maximum}$ at 2° intervals of ϕ and for $\{h, k, l\}$ = $\{400\}$, $\{220\}$, and $\{222\}$. From the special charts, values of $\overline{T}(\phi)$ were calculated and compared with values of $R(\phi)$ on the pole distribution charts. A final solution was achieved when $\overline{T}(\phi)$ and $R(\phi)$ were essentially coincident for all values of ϕ on the three $R(\phi)$ versus ϕ plots.

This method of presenting the data is, in effect, an inverse pole figure or axis distribution chart which shows the orientation distribution of the reference axis (whether it is normal, rolling, transverse, or fiber) with respect to the standard crystallographic axes. The conventional pole figure, on the other hand, indicates the orientation distribution of the diffracting plane poles with respect to reference axis and is inherently more difficult to interpret. Although this technique of preparing inverse pole figures was developed for fiber textures, it has been successfully adopted for sheet textures by treating normal, transverse, and rolling directions essentially as three separate fiber axes.

CHAPTER V

RESULTS AND DISCUSSION

The as-fabricated microstructures of the four specimens for which textures were determined are presented in Figures 7, 8, 9, and 10. Figure 7 shows the microstructure of pure aluminum indicating deformation bands typical of a severely cold-worked metal. Figure 8 illustrates the microstructure of the 5 weight per cent uranium-aluminum alloy after cold rolling indicating the density of the dispersed UAl_4 phase. The extent of dispersion is similarly characterized for the 13 weight per cent uranium-aluminum alloy, both cold rolled and extruded, in Figures 9 and 10. Microscopic inhomogeneity is quite apparent in the extruded alloy of Figure 10.

Texture data for the aluminum sample, cold rolled to a 90 per cent reduction in thickness, are illustrated in Figures 11, 12, 13, and 14. $R(\phi)$ versus ϕ charts for $\{h, k, l\} = \{222\}$, $\{002\}$, and $\{004\}$ are shown for the rolling direction in Figure 11 and the normal direction in Figure 12. Since the $R(\phi = 0)$ values for the rolling direction obtained in the present work were virtually identical with those reported by Jetter, McHargue, and Williams,[11] only a few points on the pole distribution plots were checked by calculating $\overline{T}(\phi)$. Excellent agreement between experimental values of $R(\phi)$ and the calculated values of $\overline{T}(\phi)$ can be observed. Values of $R(\phi = 0)$ for the normal direction were significantly different from those reported by the same authors.

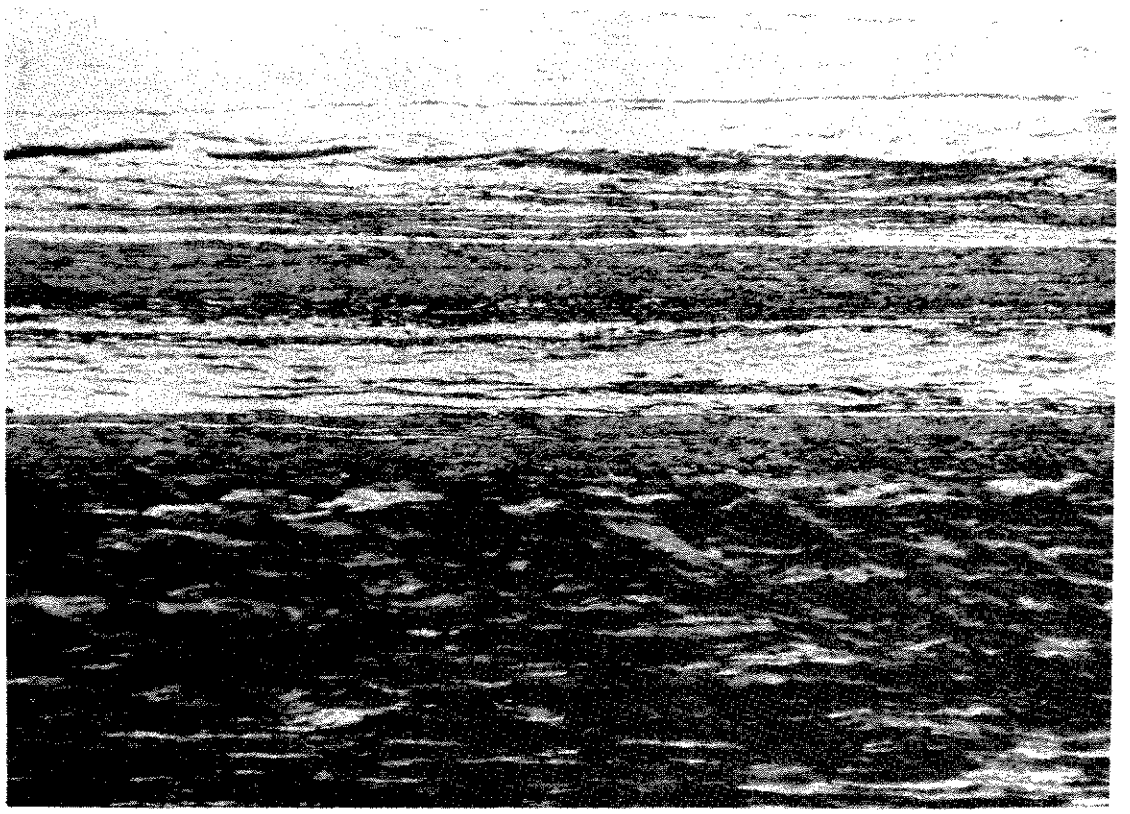

Figure 7 (Y-21460) Microstructure of high-purity aluminum cold rolled to a 90 per cent reduction in thickness. Longitudinal section photographed with sensitive tint illumination. Etchant: Electrolytic polish-etch with $HClO_4$ and C_2H_5OH. 200X.

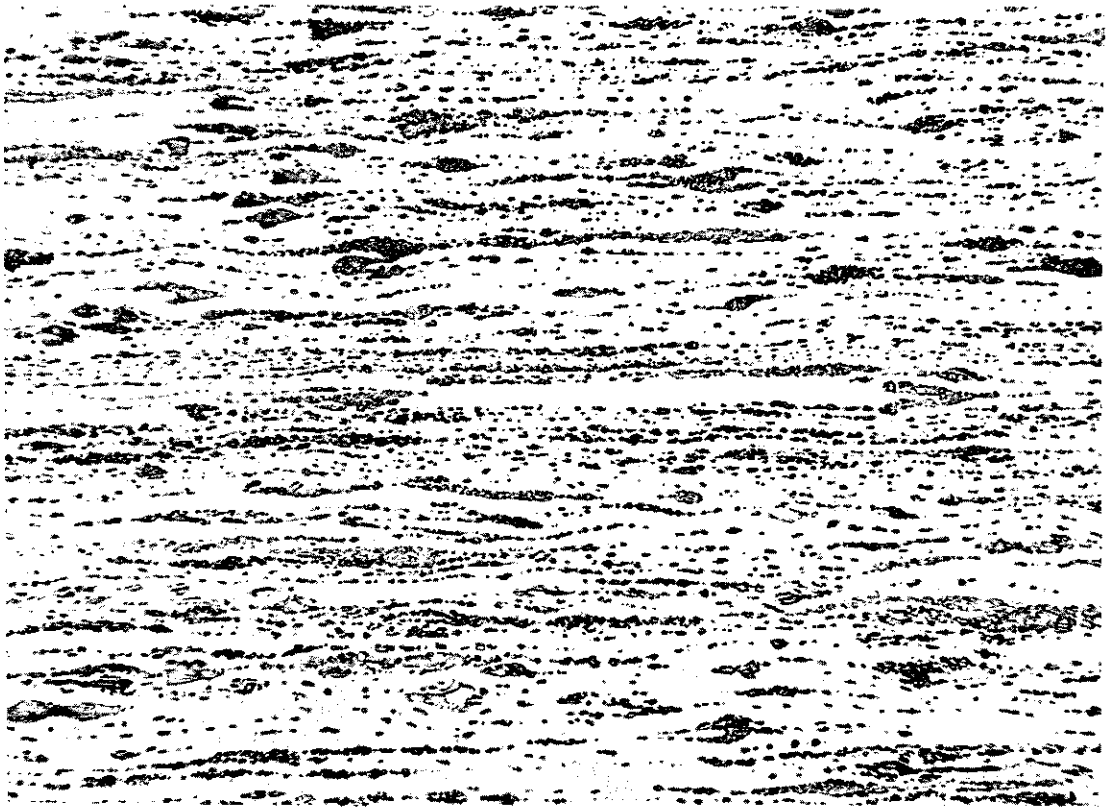

Figure 8 (Y-21459) Microstructure of 5 weight per cent uranium-aluminum alloy cold rolled to a 90 per cent reduction in thickness. Longitudinal section showing UAl_4 dispersed in an aluminum matrix. Etchant: Electrolytic polish-etch with $HClO_4$ and C_2H_5OH. 200X.

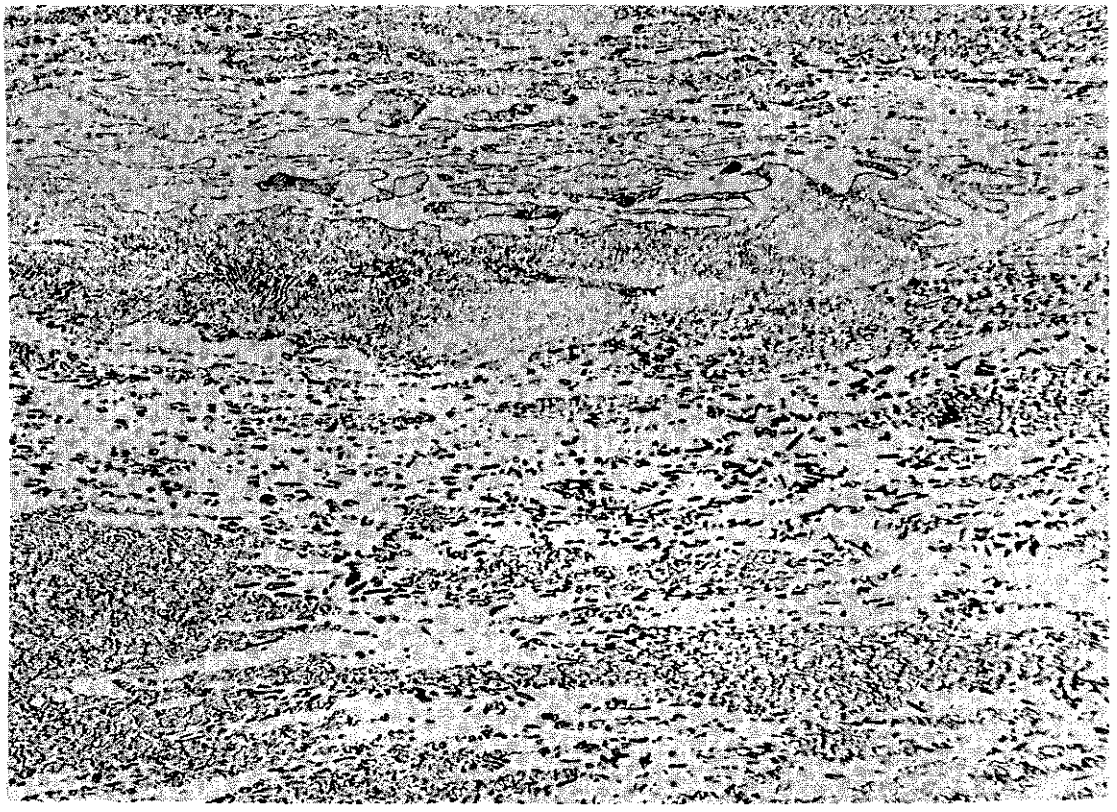

Figure 9 (Y-21864) Microstructure of 13 weight per cent uranium-aluminum alloy cold rolled to a 90 per cent reduction in thickness. Longitudinal section showing UAl_4 dispersed in an aluminum matrix. Etchant: Electrolytic polish-etch with $HClO_4$ and C_2H_5OH. 200X.

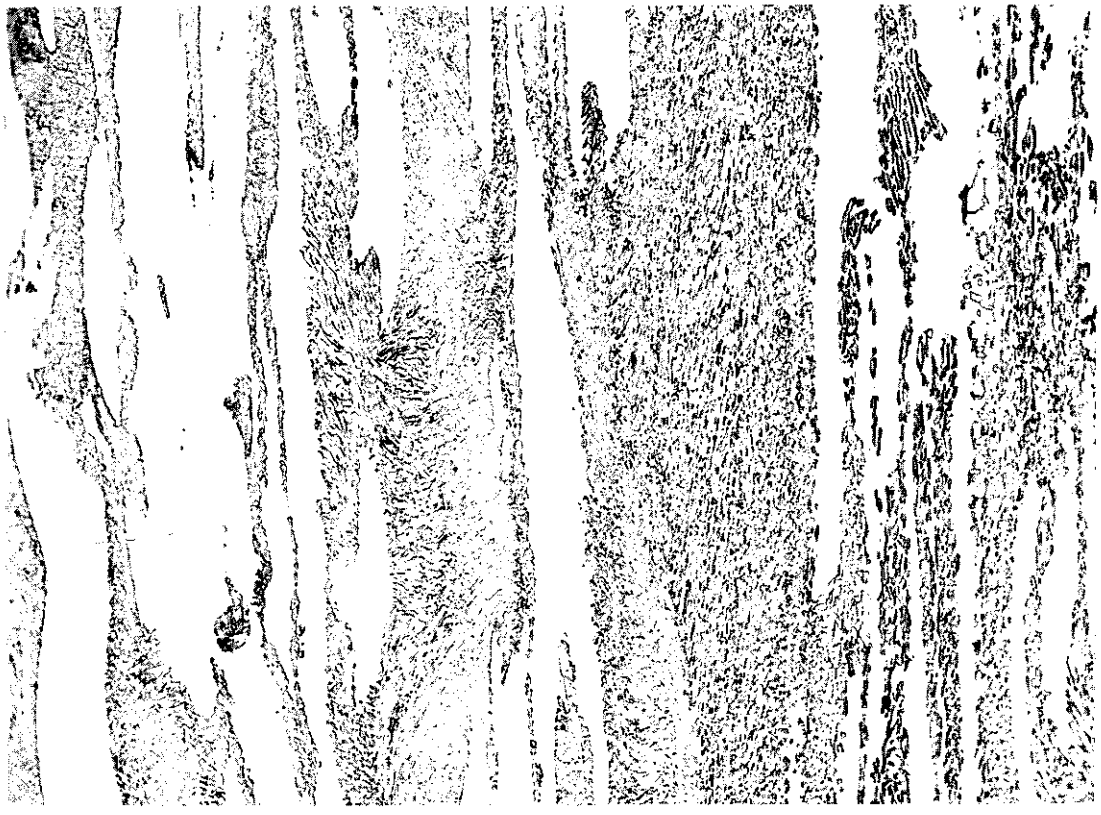

Figure 10 (Y-25589) Microstructure of 13 weight per cent uranium-aluminum alloy extruded at 455°C to a 90 per cent reduction in area. Longitudinal section showing UAl_4 dispersed in an aluminum matrix. Etchant: Electrolytic polish-etch with $HClO_4$ and C_2H_5OH. 200X.

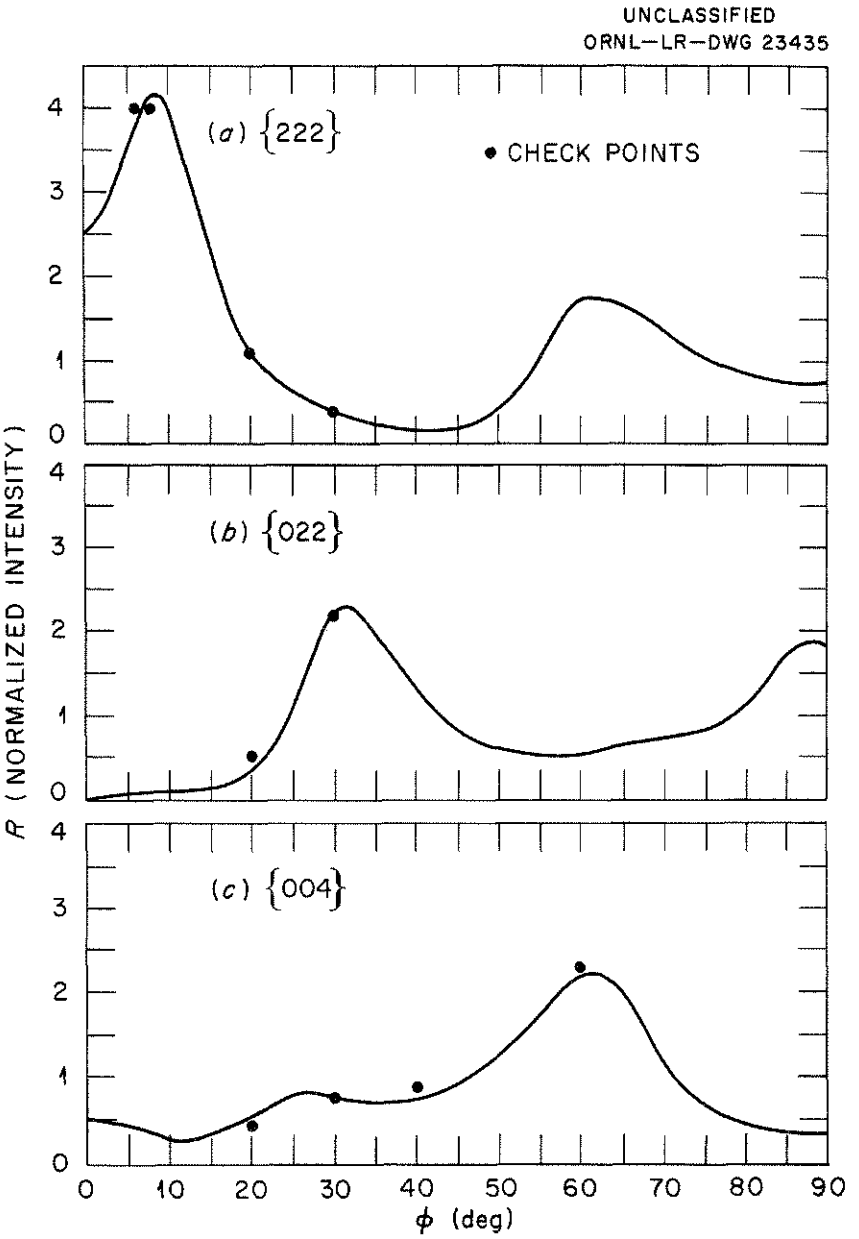

Figure 11. Pole distribution charts; aluminum — rolling direction.

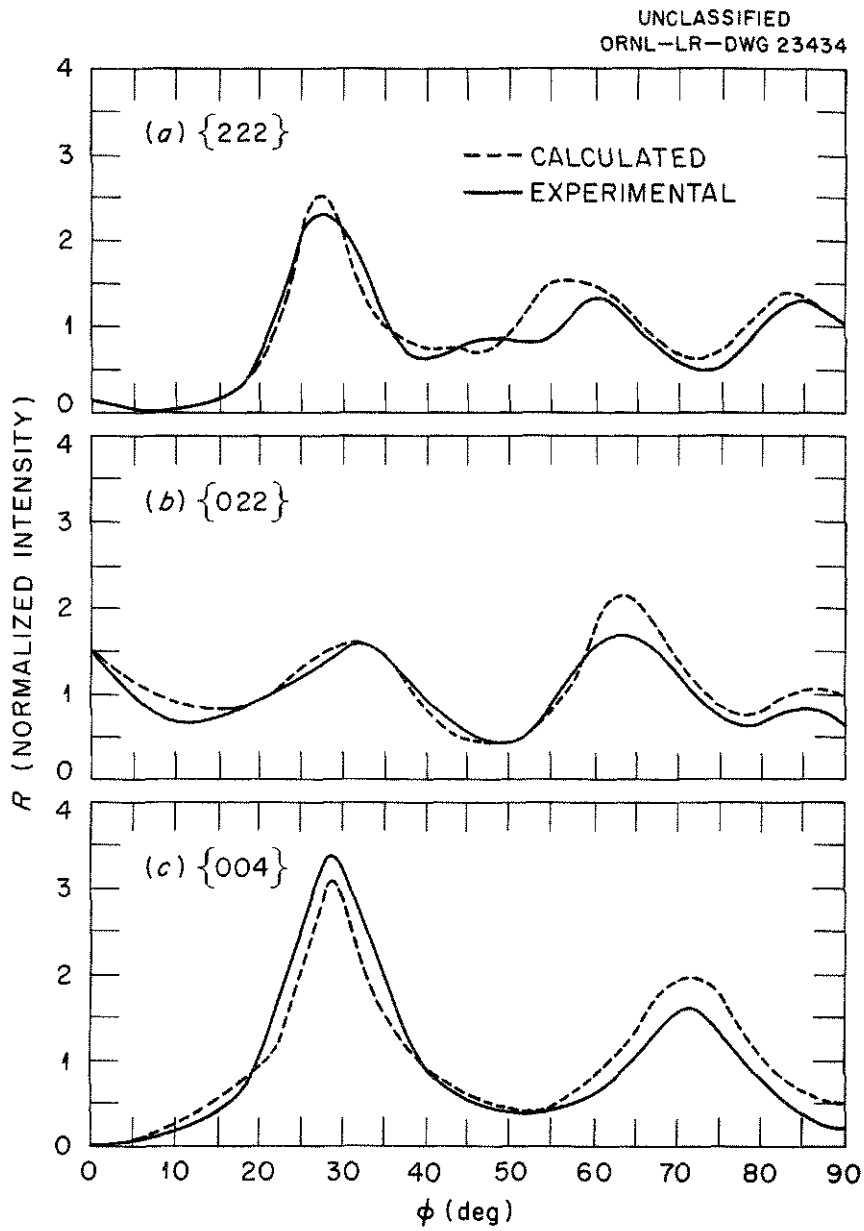

Figure 12. Pole distribution charts; aluminum – normal direction.

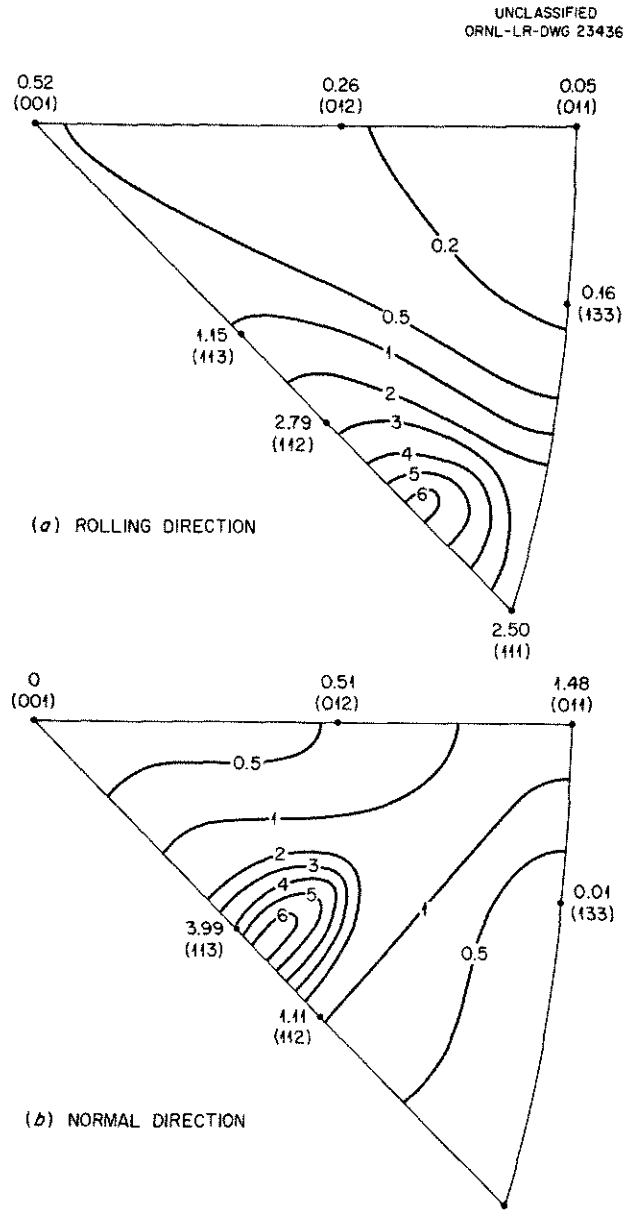

Figure 13. Axis distribution charts; aluminum – cold rolled 90 per cent.

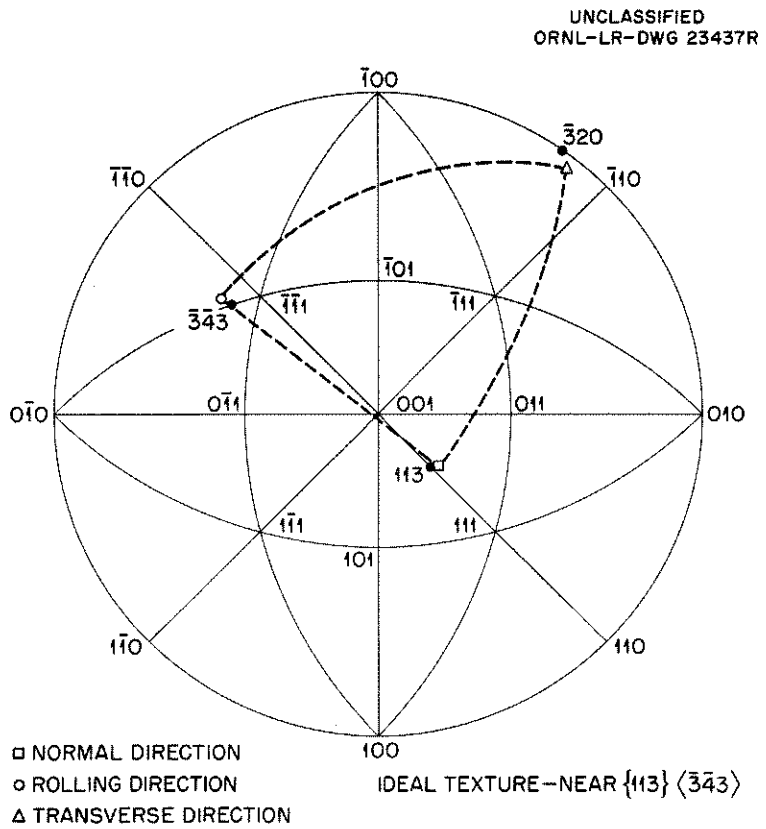

Figure 14. Aluminum — cold rolled 90 per cent.

Consequently, a comparison of $R(\phi)$ and $\overline{T}(\phi)$ was made for all values ϕ with the obtained correlation indicated in Figure 12.

Axis distribution charts or "inverse pole figures" for the rolling and normal directions are illustrated in Figure 13. The most preferred crystallographic direction of the rolling direction is near $\langle\bar{3}\bar{4}3\rangle$. The axis distribution at first falls off symmetrically from this orientation and then asymmetrically. The normal direction can be seen to fall off rapidly and symmetrically from a preferred crystallographic direction near $\langle 113\rangle$. Location of normal, transverse, and rolling directions on the standard (001) stereographic projection is shown in Figure 14 and the ideal texture has been assigned the indices near $\{113\}\langle\bar{3}\bar{4}3\rangle$.

This ideal texture deviated by 14° in the normal direction and 14° in the rolling direction from the data presented by Jetter, McHargue, and Williams.[11] A similar comparison to the data of Hu, Sperry, and Beck[10] revealed angular differences of 10° and 23° for the normal and rolling directions, respectively.

Similar information for the 5 weight per cent uranium-aluminum alloy specimen cold rolled to a 90 per cent reduction in thickness is presented in Figures 15, 16, 17, and 18. The agreement obtained between the experimental values of normalized intensity, $R(\phi)$, and the calculated values of normalized axis density, $\overline{T}(\phi)$, for all values of ϕ from 0 to 90° is shown in the pole distribution charts of Figures 15 and 16. From the axis distribution charts for this alloy, illustrated in Figure 17, it can be discerned that the intensity maxima

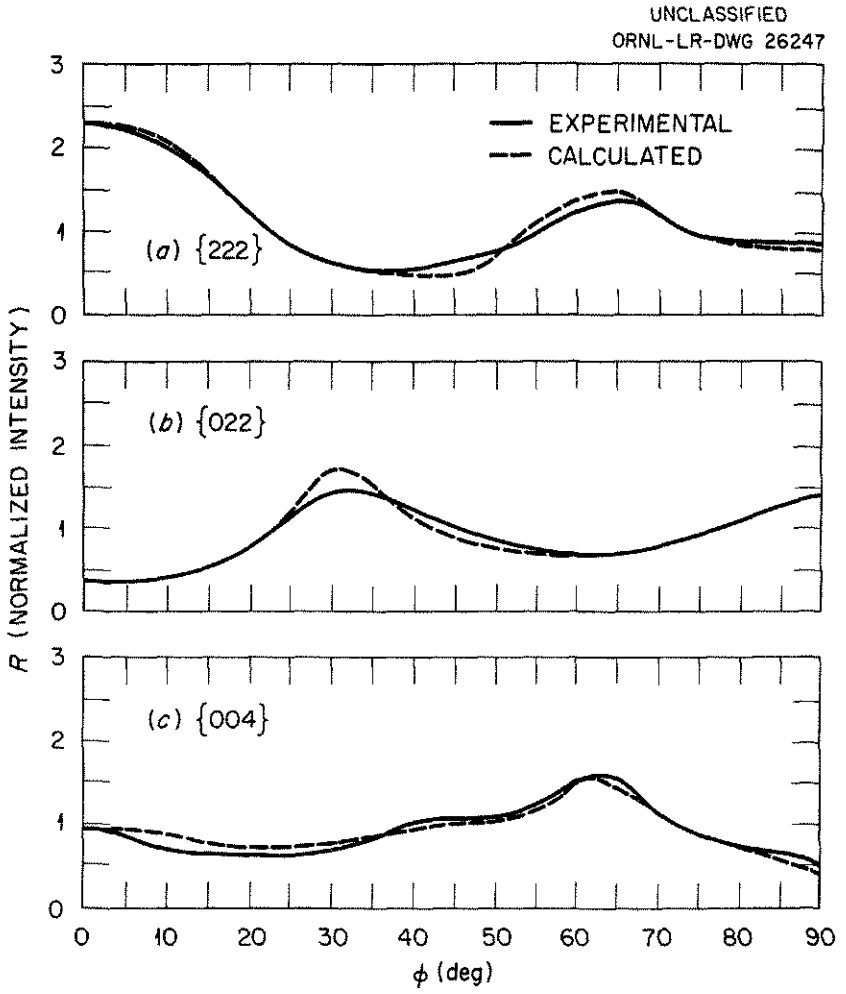

Figure 15. Pole distribution charts; 5 weight per cent uranium-aluminum alloy – rolling direction.

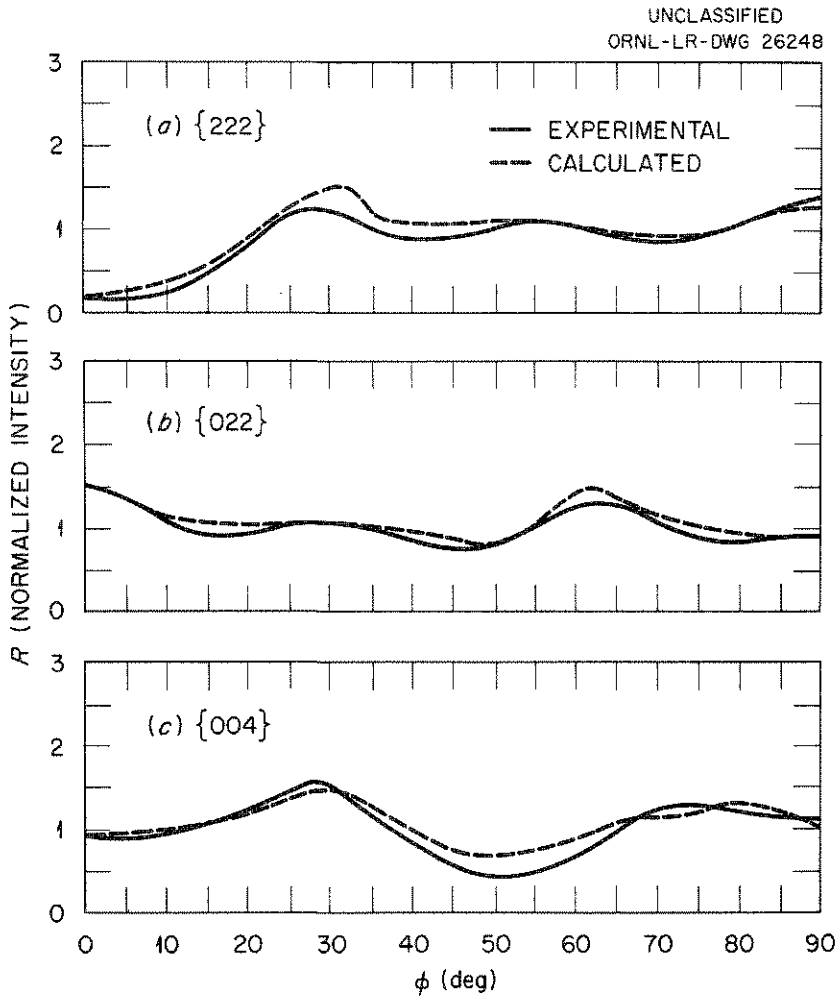

Figure 16. Pole distribution charts; 5 weight per cent uranium-aluminum alloy – normal direction.

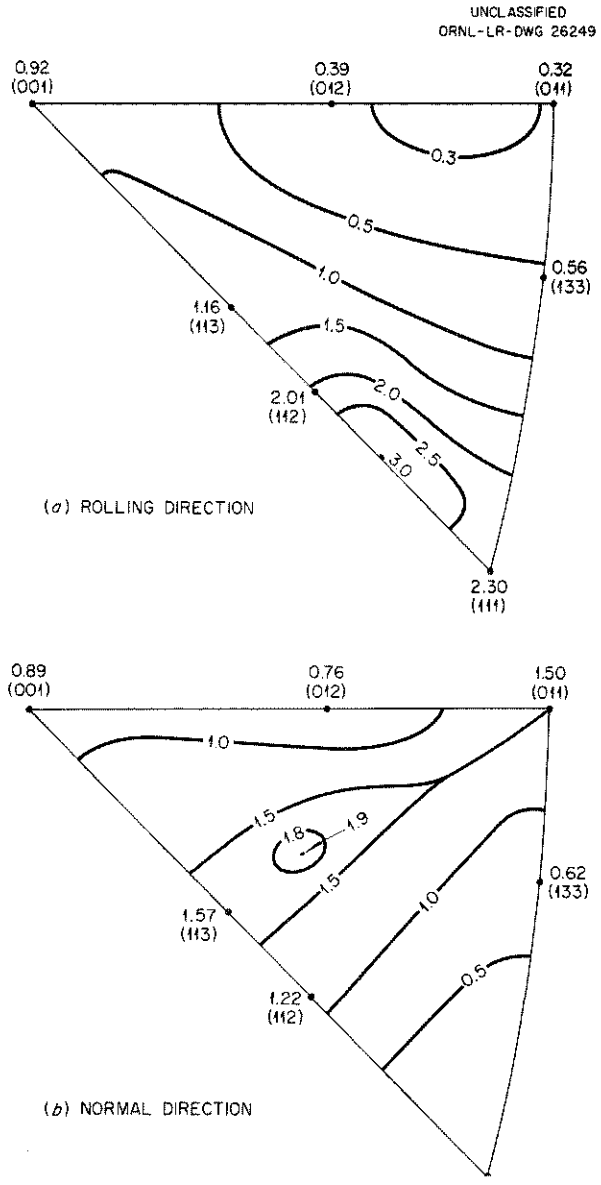

Figure 17. Axis distribution charts; 5 weight per cent uranium-aluminum alloy – cold rolled 90 per cent.

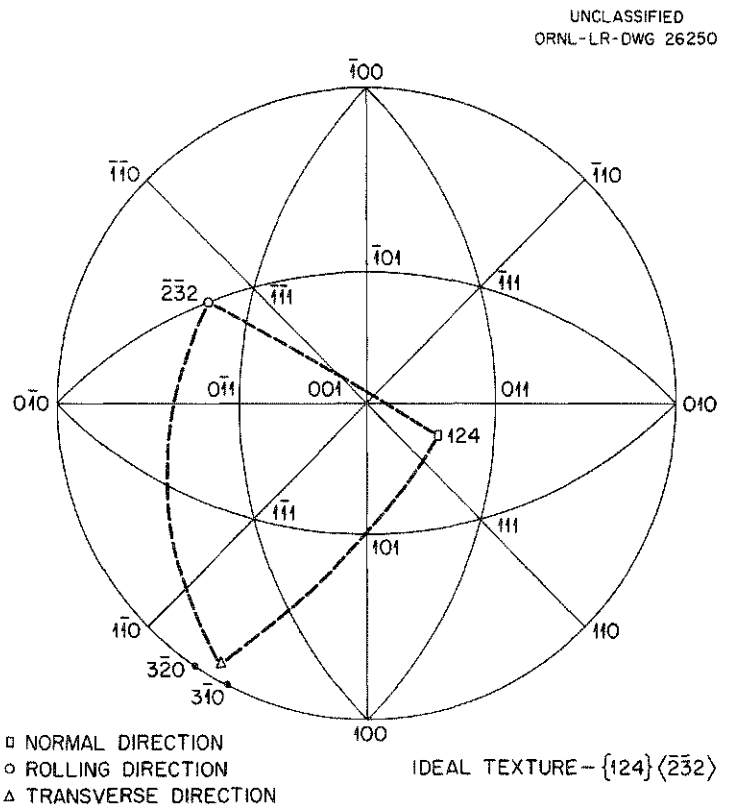

Figure 18. Five weight per cent uranium-aluminum alloy – cold rolled 90 per cent.

associated with the most preferred crystallographic directions of the rolling and normal directions are reduced by about 50 per cent and 65 per cent, respectively, from the pure aluminum specimen indicating a trend toward a more random texture. The rolling direction was found to be coincident with the $\langle\bar{2}\bar{3}2\rangle$ direction and, as such, represents a shift of 3.5° from the rolling direction for the pure aluminum specimen. The rolling plane shifted from the location near $\{113\}$ for pure aluminum to a point well within the stereographic triangle having the indices $\{124\}$. It may also be discerned from the axis distribution chart for the normal direction that the most preferred crystallographic direction is not very sharply defined but rather evidence of a band of preferred orientations is beginning to appear. The ideal texture for this alloy is located on the standard projection in Figure 18 and has been assigned the indices $\{124\}\langle\bar{2}\bar{3}2\rangle$.

Pertinent information on the orientation studies for the 13 weight per cent uranium-aluminum alloy, cold reduced to a 90 per cent reduction in thickness, is included in Figures 19, 20, 21, and 22. Pole distribution charts for this specimen, shown in Figures 19 and 20, indicate further trending toward a random texture [that is, $R(\phi) = 1$]. The reasonable agreement obtained between experimental measurements of $R(\phi)$ and calculated values of $\overline{T}(\phi)$ is also apparent. No correlation between $R(\phi)$ and $\overline{T}(\phi)$ was attempted for the normal direction trace of the $\{004\}$ because of interferences from UAl_4 diffraction which led to inconsistent values of $R(\phi = 0)$. The axis distribution charts for this specimen are shown in Figure 21. The rolling direction falls off

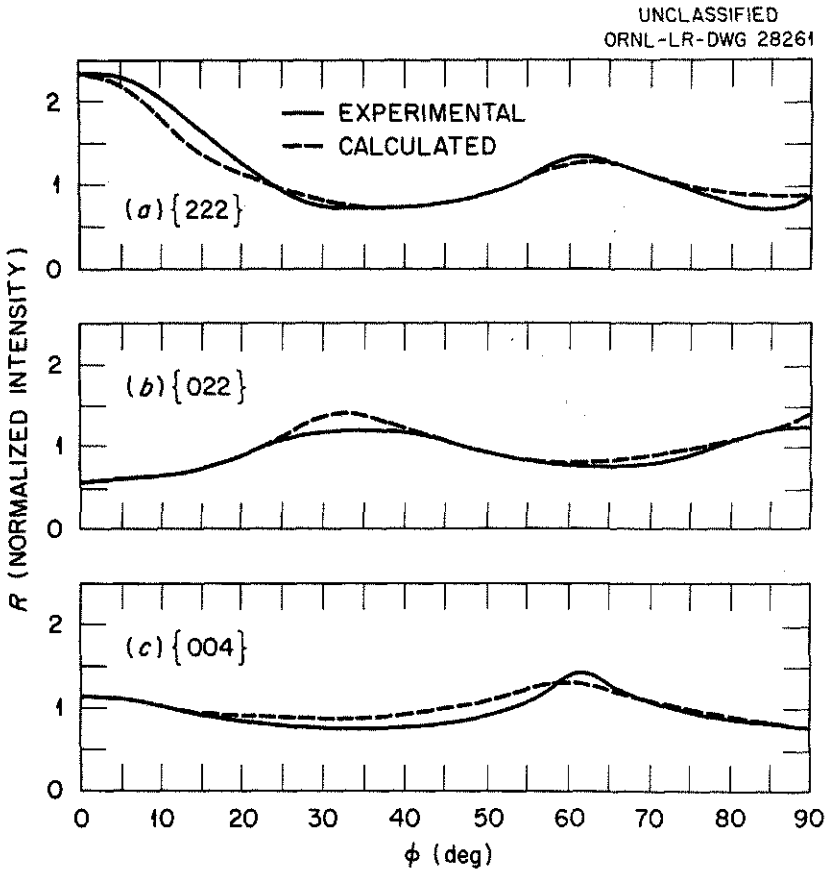

Figure 19. Pole distribution charts; 13 weight per cent uranium-aluminum alloy – rolling direction.

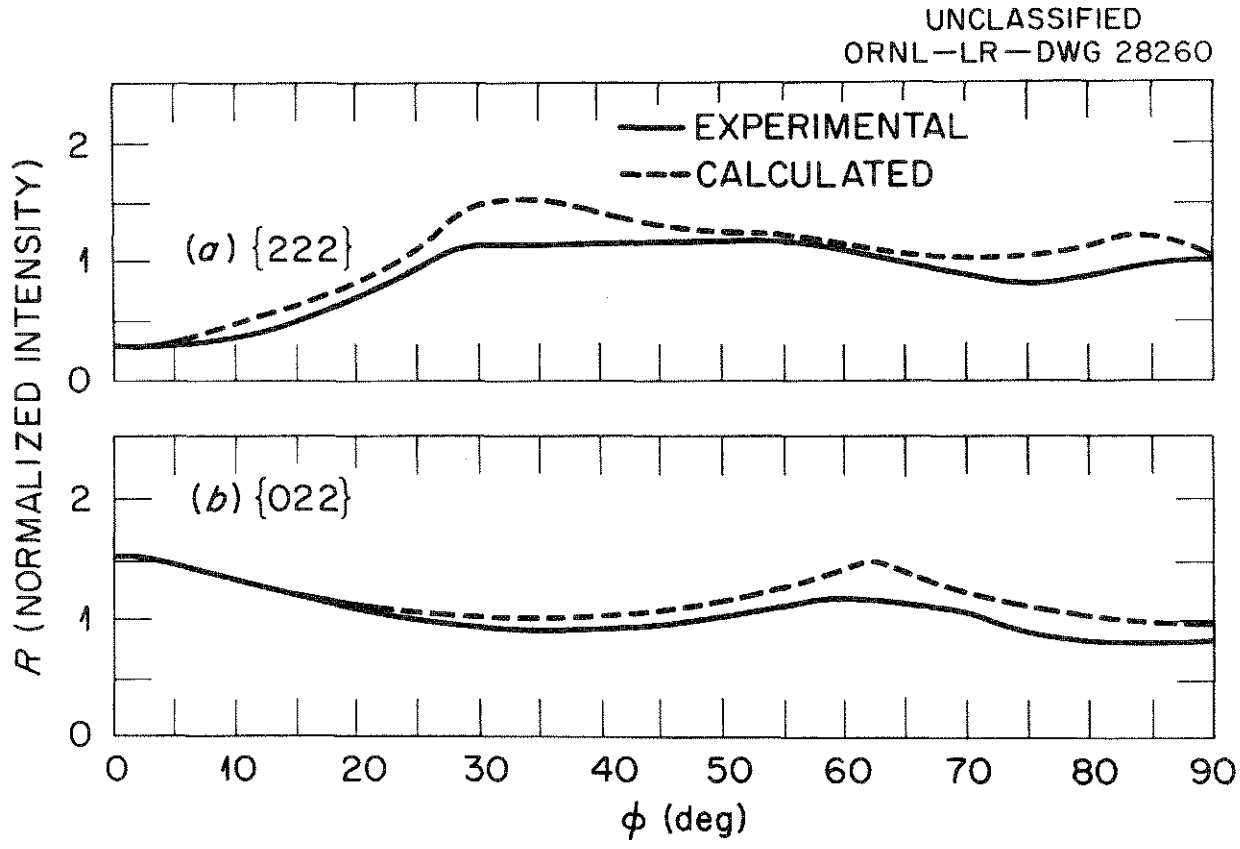

Figure 20. Pole distribution charts; 13 weight per cent uranium-aluminum alloy – normal direction.

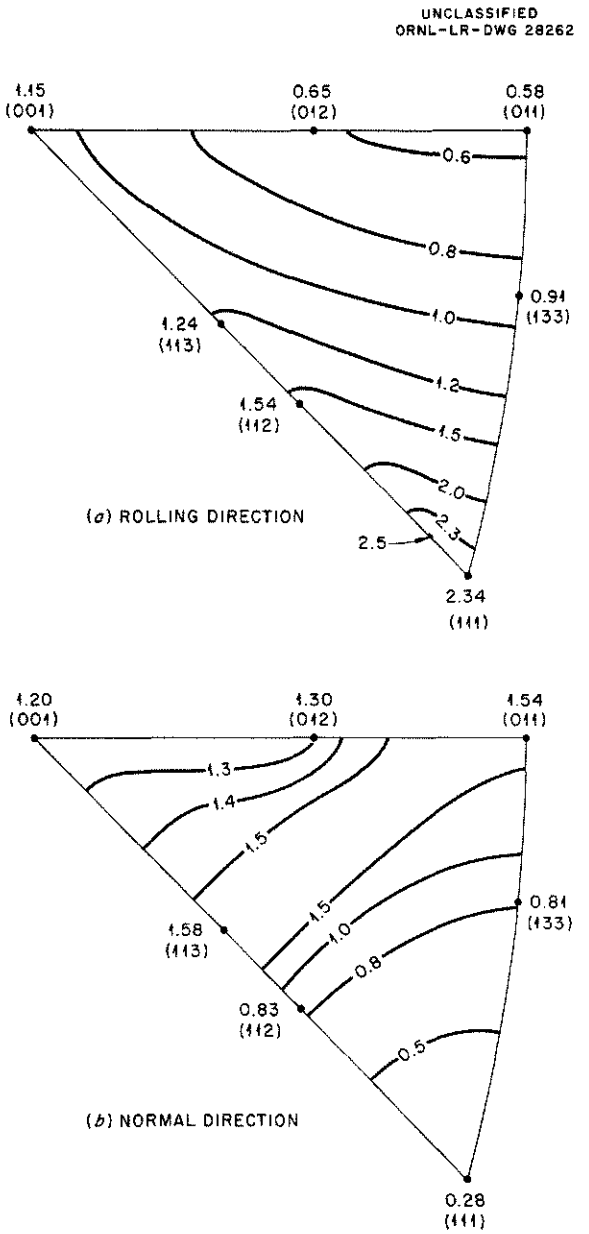

Figure 21. Axis distribution charts; 13 weight per cent uranium-aluminum alloy – cold rolled 90 per cent.

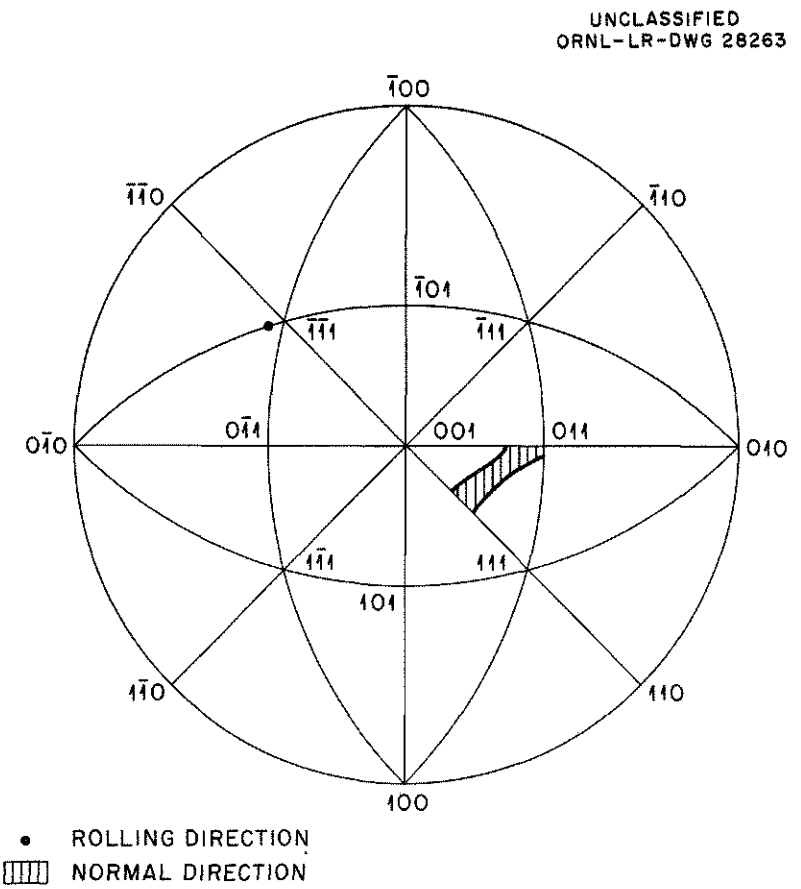

Figure 22. Thirteen weight per cent uranium-aluminum alloy — cold rolled 90 per cent.

gradually and asymmetrically from the most preferred direction which lies on the <$\bar{1}$10> zone about 4° from the <111>. The normal direction does not exhibit a single preferred crystallographic orientation but rather an equally preferred band of orientation exists precluding the possibility of specifically locating this direction. In profile the intensity contours have the following appearance indicating more clearly the asymmetry of the band.

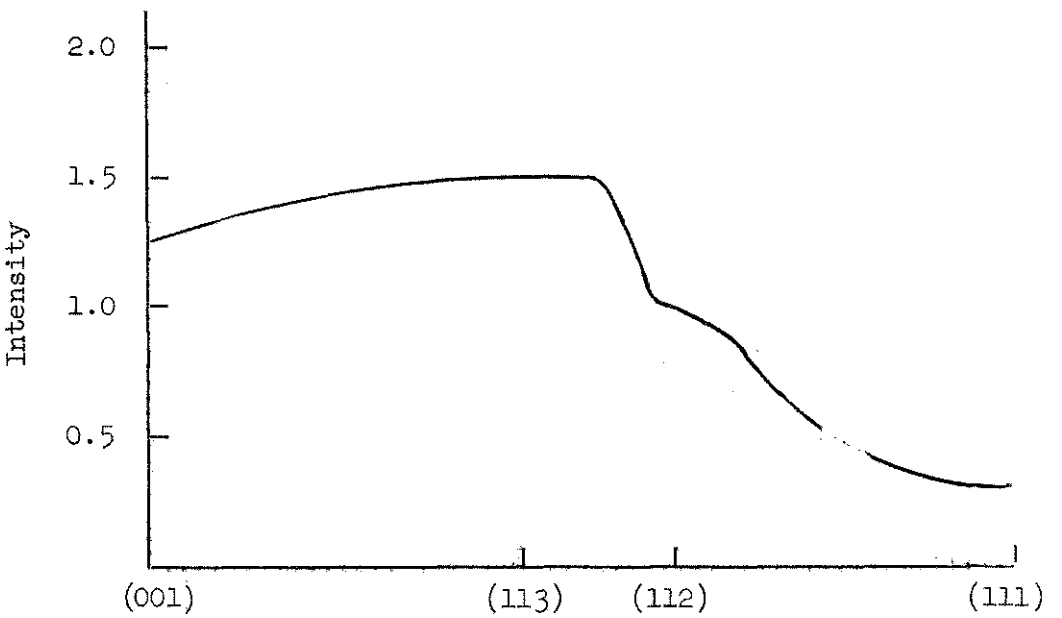

Evidence of the increasing tendency toward smearing of a single preferred rolling plane into a band of equally preferred planes or, more accurately, prevention of initial orientations from rotating into a single preferred orientation can be seen by comparing Figures 13, 17, and 21. The culmination of this process is achieved in the 13 weight per cent uranium-aluminum alloy in which the observed texture is identical to a fiber texture having a single rolling direction and an

infinite number of equally preferred normal directions which lie on the zone 90° from the rolling direction.

As a mechanistic explanation for this observation, it is suggested that during the initial stages of rolling the UAl_4 particles become aligned with the rolling plane and that areas of relatively undisturbed aluminum exist between these areas of high compound density. Evidence of this can be seen in Figure 9. The aluminum is then virtually extruded between the areas rich in UAl_4 which form the "extrusion dies". The resultant deformation texture is a fiber texture typical of extruded metals.

The rolling and normal directions for this specimen are located on the standard stereographic projection in Figure 22. Because the normal direction could not be finitely located, no attempt was made to position the transverse direction. The ideal texture is near <111>.

Finally, let us consider the 13 weight per cent uranium-aluminum alloy which was extruded into rod at 455°C with a 90 per cent reduction in area. Pole distribution charts for the fiber axis are shown in Figure 23, indicating as before the agreement between experimental and calculated intensity distributions. It can be seen that the maximum intensity was significantly greater than for the same alloy deformed by cold rolling, and a sharply defined <111> texture can be discerned from the axis distribution chart shown in Figure 24.

This texture was compared with that observed for pure aluminum extruded under similar conditions as determined by Jetter and McHargue[8] and discussed previously in Chapter III. The pure aluminum specimen,

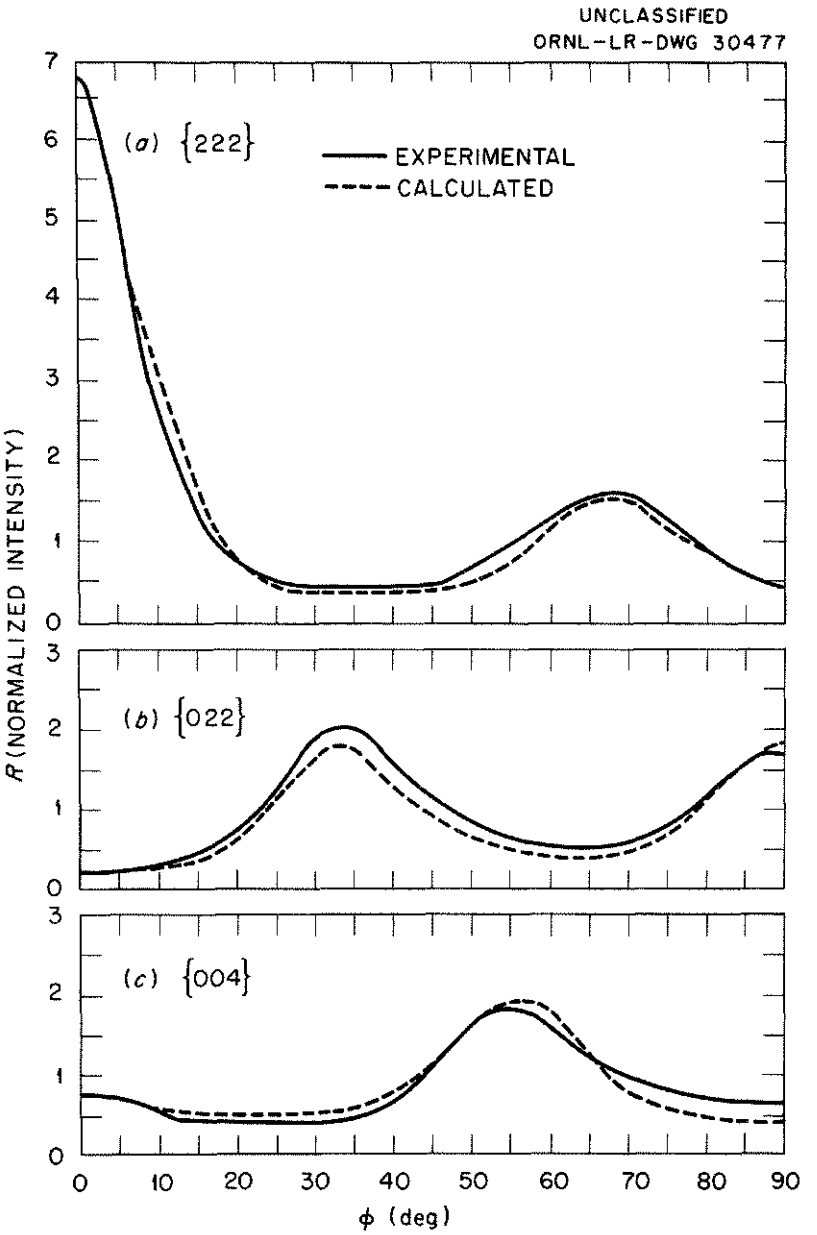

Figure 23. Pole distribution charts; 13 weight per cent uranium-aluminum alloy – extruded 90 per cent at 455°C.

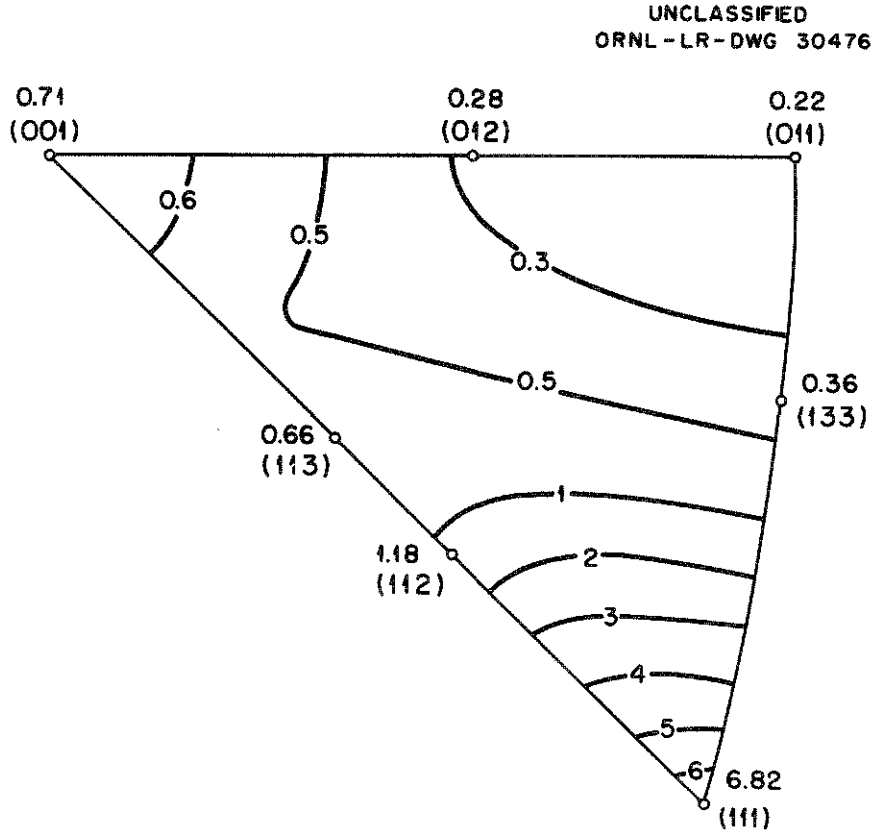

Figure 24. Axis distribution chart; 13 weight per cent uranium-aluminum alloy – extruded 90 per cent at 455°C.

it will be remembered, had a duplex fiber texture consisting of 22 per cent <111>, the deformation component, and 78 per cent <100>, the recrystallization component. The uranium-aluminum alloy specimen contained essentially no <100>. However, examination of the microstructure of the alloy revealed essentially complete recrystallization as would, of course, be predicted from knowledge that the extrusion temperature was high relative to the accepted recrystallization temperature for aluminum. Metallographic evidence of recrystallization can be found in Figure 25. Further evidence that the <111> was aligned with the fiber axis was obtained by etch pitting a transverse section of the uranium-bearing alloy. Triangular etch pits characteristic of <111> can be clearly seen in Figure 26. For comparison, the microstructure of pure aluminum, similarly extruded, is included in Figure 27. In this figure, the triangular etch pits representative of <111> deformation component are visible in the deformed grains while the square etch pits characteristic of the <100> recrystallization component can be seen in the equiaxed recrystallized grains.

The question naturally arises – "Why does pure aluminum contain the <100> recrystallization component while a 13 weight per cent uranium-aluminum alloy, similarly extruded, contains <111> as the recrystallization component?" Unfortunately, the present state of development of deformation and recrystallization texture theory precludes offering any but superficial explanations to this perplexing question. It is obvious, however, that the presence of the dispersed phase alters the manner in which lattice rotations occur.

Fig. 25 (Y-26380) Microstructure of 13 weight per cent uranium-aluminum alloy extruded to a 90 per cent reduction in area at 455°C. Transverse section photographed with slightly oblique illumination to delineate grains in the areas of pure aluminum which recrystallized during extrusion. Etchant: Electropolished and anodized. 750X.

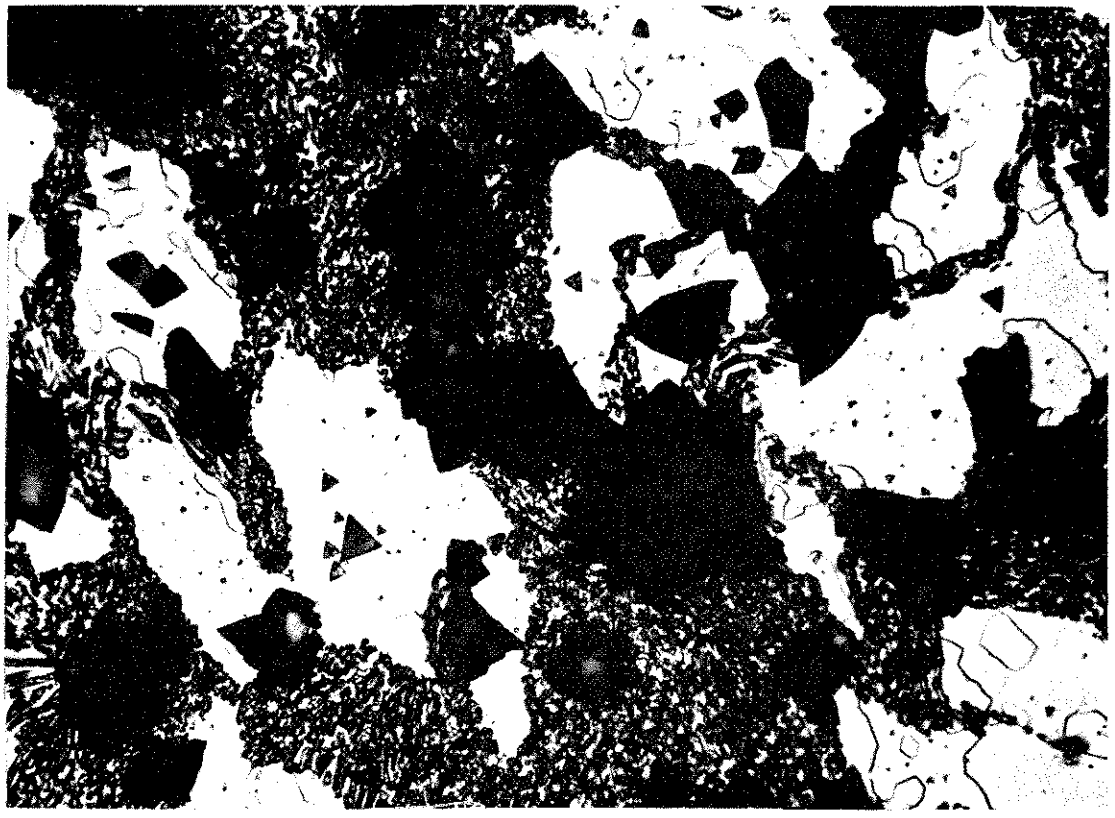

Fig. 26 (Y-26381) Microstructure of 13 weight per cent uranium-aluminum alloy extruded to a 90 per cent reduction in area at 455°C. Transverse section prepared to reveal triangular etch pits in areas of pure aluminum indicating {111} texture in recrystallized grains. Etchant: Aqueous solution of HF, HCl, and HNO_3. 750X.

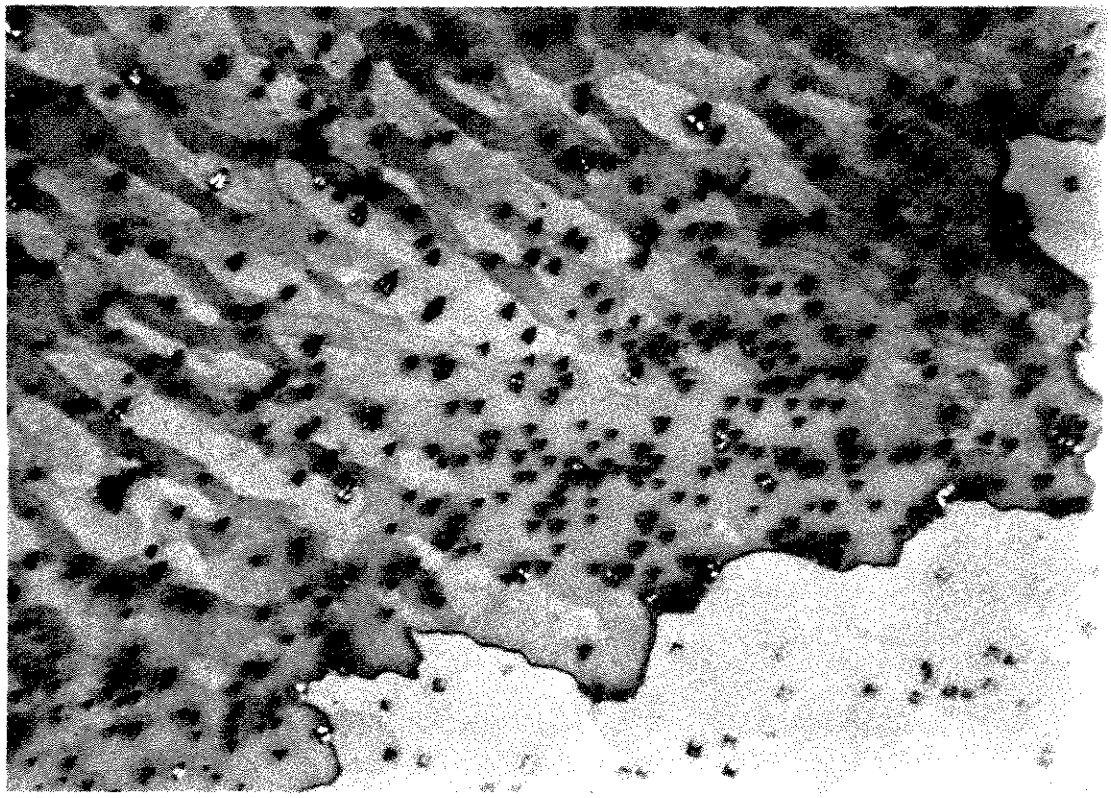

Fig. 27 (Y-14676) Microstructure of high-purity aluminum extruded to a 90 per cent reduction in area at 455°C. Transverse section prepared to reveal etch pits. Triangular etch pits in grain with numerous deformation bands are typical of {111} texture while square etch pits in deformation-free grain are typical of {100} recrystallization texture occurring during extrusion.
Etchant: Aqueous solution of HF, HCl, and HNO_3. 500X.

CHAPTER VI

CONCLUSIONS

1. Alloys containing increasing amounts of the dispersed phase, UAl_4, exhibit an increasing tendency toward random orientation as expected, since the dispersed phase prevents normal lattice rotations from occurring.

2. The rolling direction in each of the three cold-rolled samples was found to lie along the $\langle\bar{1}10\rangle$ zone and the maximum angular variation between the specimens was only 7.5°. It is, therefore, concluded that the presence of a dispersed phase produces no appreciable shift in the rolling direction.

3. In the cold-rolled uranium-bearing specimens, impedance of lattice rotations is manifested by the formation of a broad band of equally preferred orientations for the normal direction rather than a single crystallographic direction aligned with the normal direction. This close similarity to a fiber texture is attributed to the fact that the dispersed phase becomes aligned with the rolling plane during the initial stages of deformation and the aluminum matrix is subsequently forced between these particles in much the same manner as if the alloy were being extruded.

4. The ideal textures for pure aluminum and the 5 weight per cent uranium-aluminum alloy reduced 90 per cent in thickness by cold rolling are near $\{113\}\langle\bar{3}\bar{4}3\rangle$ and $\{124\}\langle\bar{2}\bar{3}2\rangle$, respectively. The ideal

orientation for the 13 weight per cent uranium-aluminum alloy, similarly fabricated, is essentially a near <111> fiber texture.

5. The fiber texture of a 13 weight per cent uranium-aluminum alloy extruded at 455°C to a 90 per cent reduction in area is <111>. Although this specimen had undergone essentially complete recrystallization during extrusion, little evidence of the <100> component could be found indicating that lattice rotations normally occurring during recrystallization are prevented by the presence of the dispersed phase.

LIST OF REFERENCES

1. Boas, W. and Schmid, E., "Interpretation of Deformation Textures," Z. tech. Phys., 12, 71 (1931)

2. Pickus, M. R. and Mathewson, C. H., "On the Theory of the Origin of Rolling Textures in Face-Centered Cubic Metals," J. Inst. Metals, 64, 237 (1939)

3. Hibbard, W. R. and Yen, M. K., "Wire Textures in Copper and Its Binary Alpha Solid Solution Alloys with Aluminum, Nickel, and Zinc," Trans. Am. Inst. Mining and Met. Engrs., 175, 126 (1948)

4. Calnan, E. A. and Clews, C. J. B., "Deformation Textures in Face-Centered Cubic Metals," Phil. Mag., 41, 1085 (1950)

5. Schmid, E. and Wasserman, G., "Concerning the Textures in Hard-Drawn Wires," Z. Physik, 42, 779 (1927)

6. Hibbard, W. R., "Deformation Texture of Drawn Face-Centered Cubic Metal Wires," J. Inst. Metals, 77, 58 (1950)

7. Barrett, C. S., Structure of Metals, Chapters XV, XVII, XVIII, and XIX (New York: McGraw-Hill Book Company, 1950)

8. McHargue, C. J. and Jetter, L. K., Oak Ridge National Laboratory, Unpublished Information

9. Dahl, O. and Pawlek, F., "Preferred Orientation and Grain Growth in Rolled Plate," Z. Metallkunde, 28, 266 (1936)

10. Hu, H., Sperry, P. R., and Beck, P. A., "Rolling Textures in Face-Centered Cubic Metals," Trans. Am. Inst. Mining and Met. Engrs., 194, 76 (1952)

11. Jetter, L. K., McHargue, C. J., and Williams, R. O., "Method of Representing Preferred Orientation Data," J. Appl. Phys., 27, 374 (1956)

12. Smallman, R. E. and Westmacott, K. H., Textures in Face-Centered Cubic Metals and Alloys, AERE-M/R-1603 (1955)

13. Brick, R. M., "Deformation Textures," Cold-Working of Metals (Cleveland: Am. Soc. Metals, 1949) p. 105

14. Jetter, L. K. and Borie, B. S., Jr., "A Method for the Quantitative Determination of Preferred Orientations," J. Appl. Phys., 24, 532-535 (1953)

ORNL-2635
Metallurgy and Ceramics
TID-4500 (14th ed.)

INTERNAL DISTRIBUTION

1. C. E. Center
2. Biology Library
3. Health Physics Library
4. Metallurgy Library
5-6. Central Research Library
7. Reactor Experimental Engineering Library
8-27. Laboratory Records Department
28. Laboratory Records, ORNL R. C.
29. A. M. Weinberg
30. L. B. Emlet (K-25)
31. J. P. Murray (Y-12)
32. J. A. Swartout
33. E. H. Taylor
34. E. D. Shipley
35. M. L. Nelson
36. W. H. Jordan
37. C. P. Keim
38. R. S. Livingston
39. R. R. Dickison
40. S. C. Lind
41. F. L. Culler
42. A. H. Snell
43. A. Hollaender
44. M. T. Kelley
45. K. Z. Morgan
46. J. A. Lane
47. A. S. Householder
48. C. S. Harrill
49. D. S. Billington
50. C. E. Winters
51. H. E. Seagren
52. D. Phillips
53. A. J. Miller
54. R. A. Charpie
55. C. F. Leitten
56. E. G. Bohlmann
57. M. J. Skinner
58. C. O. Smith
59. J. H. Frye, Jr.
60. W. W. Parkinson
61. W. D. Manly
62. J. E. Cunningham
63. G. M. Adamson, Jr.
64. J. W. Allen
65. R. J. Beaver
66. E. S. Bomar, Jr.
67. R. E. Clausing
68. J. H. Coobs
69. J. H. DeVan
70. L. M. Doney
71. D. A. Douglas, Jr.
72. E. A. Franco-Ferreira
73. R. J. Gray
74. J. P. Hammond
75. R. L. Heestand
76. T. Hikido
77-111. M. R. Hill
112. E. E. Hoffman
113. H. Inouye
114. L. K. Jetter
115. C. J. McHargue
116. P. Patriarca
117. M. L. Picklesimer
118. T. K. Roche
119. G. P. Smith, Jr.
120. A. Taboada
121-130. W. C. Thurber
131. R. C. Waugh
132. E. E. Stansbury (consultant)
133. W. O. Harms (consultant)
134. J. H. Keonig (consultant)
135. H. Leidheiser, Jr. (consultant)
136. C. S. Smith (consultant)
137. H. A. Wilhelm (consultant)
138. ORNL - Y-12 Technical Library, Document Reference Section

EXTERNAL DISTRIBUTION

139. D. E. Baker, General Electric Company, Hanford
140. E. Evans, General Electric Company, Hanford
141. Division of Research and Development, AEC, ORO
142-625. Given distribution as shown in TID-4500 (14th ed.) under Metallurgy and Ceramics category

Central
Research Library
Document Collection

NOV 6 1958